bioRxiv preprint doi: https://doi.org/10.1101/374488; this version posted July 23, 2018. The copyright holder for this preprint (which was not certified by peer review) is the author/funder, who has granted bioRxiv a license to display the preprint in perpetuity. It is made available under aCC-BY-NC 4.0 International license.

EIPR1 controls dense-core vesicle cargo sorting and EARP complex localization in insulinoma cells

Irini Topalidou[*†], Jérôme Cattin-Ortolá[*†], Michael Ailion[*]

[*]Department of Biochemistry, University of Washington, Seattle, WA 98195

[†]These authors contributed equally to this work

bioRxiv preprint doi: https://doi.org/10.1101/374488; this version posted July 23, 2018. The copyright holder for this preprint (which was not certified by peer review) is the author/funder, who has granted bioRxiv a license to display the preprint in perpetuity. It is made available under aCC-BY-NC 4.0 International license.

Running Title: EARP is required for insulin secretion

Key words: EARP complex, dense-core vesicles, GARP complex, insulin, endosomes.

Corresponding author:

Michael Ailion

Department of Biochemistry

University of Washington

Box 357350

1705 NE Pacific St

Seattle, WA 98195

Phone: 206-685-0111

email: mailion@uw.edu

bioRxiv preprint doi: https://doi.org/10.1101/374488; this version posted July 23, 2018. The copyright holder for this preprint (which was not certified by peer review) is the author/funder, who has granted bioRxiv a license to display the preprint in perpetuity. It is made available under aCC-BY-NC 4.0 International license.

Abstract

Dense-core vesicles (DCVs) are secretory vesicles found in neurons and endocrine cells. DCVs package and release cargos including neuropeptides, biogenic amines, and peptide hormones. We recently identified the endosome-associated recycling protein (EARP) complex and the EARP-interacting protein EIPR-1 as proteins important for DCV biogenesis in *C. elegans* neurons. Here we determine the role of mammalian EIPR1 in insulinoma cells. We find that in *Eipr1* KO cells, mature DCV cargos such as insulin accumulate at the trans-Golgi network and there is reduced insulin secretion. In addition, we find that EIPR1 is required for the stability of the EARP complex subunits and for the localization of EARP and its association with membranes. EARP is localized to two distinct compartments related to its function: an endosomal compartment and a DCV-related compartment. We propose that EIPR1 functions with EARP to control both endocytic recycling and DCV cargo sorting.

bioRxiv preprint doi: https://doi.org/10.1101/374488; this version posted July 23, 2018. The copyright holder for this preprint (which was not certified by peer review) is the author/funder, who has granted bioRxiv a license to display the preprint in perpetuity. It is made available under aCC-BY-NC 4.0 International license.

Introduction

Dense-core vesicles (DCVs) are regulated secretory vesicles found in neurons and endocrine cells, where they are also called secretory granules. DCVs package several types of cargos, including neuropeptides and peptide hormones, for release at the cell membrane (Gondré-Lewis et al., 2012). The secreted cargos modulate a variety of processes including development, growth, glucose metabolism, and mental state. DCVs are generated at the trans-Golgi network (TGN) in a process that includes correct sorting of cargos and acquisition of proper compartmental identity. Because DCVs are not regenerated locally at release sites, the DCV pool needs to be continuously supplied by the TGN.

Genetic studies in the nematode *C. elegans* have identified several new molecules that function in DCV biogenesis, including the endosome-associated recycling protein (EARP) complex and the EARP-interacting protein EIPR-1, a WD40 domain protein which interacts with EARP (Hannemann et al., 2012; Mesa et al., 2011; Yu et al., 2011; Topalidou et al., 2016; Ailion et al., 2014; Edwards et al., 2009; Sumakovic et al., 2009). The EARP complex is structurally similar to the Golgi-associated retrograde protein (GARP) complex. EARP shares the VPS51, VPS52, and VPS53 subunits with the GARP complex, but uses VPS50 instead of VPS54 as the fourth subunit (Gillingham et al., 2014; Schindler et al., 2015). Whereas GARP functions in retrograde transport from endosomes to the TGN (Conibear and Stevens, 2000; Conibear et al., 2003; Pérez-Victoria and Bonifacino, 2009; Pérez-Victoria et al., 2008; Perez-Victoria et al., 2010), EARP was shown to act in recycling

bioRxiv preprint doi: https://doi.org/10.1101/374488; this version posted July 23, 2018. The copyright holder for this preprint (which was not certified by peer review) is the author/funder, who has granted bioRxiv a license to display the preprint in perpetuity. It is made available under aCC-BY-NC 4.0 International license.

cargos from endosomes back to the plasma membrane (Schindler et al., 2015). In *C. elegans*, the EARP complex and EIPR1 were shown to be required for sorting cargo to DCVs (Topalidou et al., 2016). The VPS50 subunit of the EARP complex was also shown to be required for the maturation of DCV cargos and DCV acidification (Paquin et al., 2016).

Here we investigate the role of mammalian EIPR1 in DCV function and EARP complex formation using insulin-secreting insulinoma cells. EIPR1 physically interacts with the EARP complex in rat insulinoma cells (Topalidou et al., 2016). EIPR1 (also named TSSC1) was also independently identified as a physical interactor and functional partner of both the GARP and EARP complexes in human cell lines (Gershlick et al., 2016). Moreover, two mass spectrometry interactome data sets identified EIPR1 as an interactor of EARP subunits in human HEK293T and HeLa cells (Hein et al., 2015; Huttlin et al., 2015). WD40 domain proteins like EIPR1 often act as scaffolds for the assembly of protein complexes (Stirnimann et al., 2010). Though EIPR1 interacts with EARP, it has not been determined whether EIPR1 is required for the localization or stability of the EARP complex. Fluorescence recovery after photobleaching in *Eipr1* knockdown cells showed that EIPR1 is required for efficient recruitment of GARP to the TGN (Gershlick et al., 2016).

In this study we use *Eipr1* knockout and rescue experiments in insulin-secreting cells to demonstrate that EIPR1 controls proper insulin secretion and localization of mature DCV cargo. We also find that EIPR1 is required for the stability of the EARP complex subunits and for proper localization and association of EARP with membranes. Finally, we show that EARP localizes to two distinct

bioRxiv preprint doi: https://doi.org/10.1101/374488; this version posted July 23, 2018. The copyright holder for this preprint (which was not certified by peer review) is the author/funder, who has granted bioRxiv a license to display the preprint in perpetuity. It is made available under aCC-BY-NC 4.0 International license.

compartments relevant to its functions in endocytic recycling and DCV cargo sorting.

bioRxiv preprint doi: https://doi.org/10.1101/374488; this version posted July 23, 2018. The copyright holder for this preprint (which was not certified by peer review) is the author/funder, who has granted bioRxiv a license to display the preprint in perpetuity. It is made available under aCC-BY-NC 4.0 International license.

Results

EIPR1 is required for insulin secretion

We recently showed that the *C. elegans* WD40 domain protein EIPR-1 is needed for dense-core vesicle (DCV) cargo trafficking in *C. elegans* neurons (Topalidou et al., 2016). To investigate the role of EIPR1 in the trafficking of mammalian DCV cargo in endocrine cells, we generated EIPR1 knockout (KO) insulinoma 832/13 cells using the CRISPR technology by inserting a puromycin cassette in the first exon of *Eipr1* (Figure 1A and S1A). We identified positive clones by PCR (Figure S1C). To confirm that EIPR1 is lost in the *Eipr1* KO line, we analyzed the cells for EIPR1 expression by Western blot. Wild-type (WT) cells displayed a band at around 45 kD, the approximate molecular weight of EIPR1, which was missing from *Eipr1* KO cells (Figure 1B).

To examine whether EIPR1 is needed for sorting cargo to DCVs in insulinoma cells, we measured insulin secretion of WT and *Eipr1* KO cells under resting (5 mM KCl, 0 mM glucose) and stimulating (55 mM KCl, 25 mM glucose) conditions. Insulin secretion under both resting and stimulating conditions was lower in *Eipr1* KO cells than in WT cells (stimulated secretion was reduced to ~ 25% of WT, Figure 1C, left panel). To verify that the effects were due to loss of EIPR1, we introduced a wild type *Eipr1* cDNA into the *Eipr1* KO cells by lentiviral transduction (Figure 1B). Expression of wild type EIPR1 in *Eipr1* KO cells (Eipr1(+)) rescued the stimulated insulin secretion defect of the *Eipr1* KO line, confirming that this defect is due to loss of EIPR1 (Figure 1C, left panel).

bioRxiv preprint doi: https://doi.org/10.1101/374488; this version posted July 23, 2018. The copyright holder for this preprint (which was not certified by peer review) is the author/funder, who has granted bioRxiv a license to display the preprint in perpetuity. It is made available under aCC-BY-NC 4.0 International license.

Defective insulin secretion can be due to reduced insulin content. Total insulin content of *Eipr1* KO was only slightly reduced (to ~ 80% of WT, Figure 1C, middle panel), and the difference was not statistically significant. After normalizing insulin secretion to total insulin content, we found that insulin secretion under stimulating conditions is still significantly reduced in the *Eipr1* KO line (~30% of WT, Figure 1C, right panel), suggesting that the reduced insulin secretion cannot be explained by reduced total insulin levels.

The observed decrease in insulin secretion in the *Eipr1* KO could be due to a defect in the processing of proinsulin to insulin. Thus, we measured the total and secreted levels of proinsulin. Although secretion of proinsulin was not altered in *Eipr1* KO (Figure 1D, left panel), total proinsulin content was reduced (~50% of WT, Figure 1D, middle panel), but this reduction was not significantly rescued in Eipr1(+) cells. Secretion of proinsulin was similar in resting and stimulating conditions, suggesting that its release is independent of the regulated secretory pathway. When normalized to total proinsulin content, the *Eipr1* KO had increased proinsulin secretion compared to WT (Figure 1D, right panel), but the difference was not statistically significant. Similarly, the ratio of total cellular proinsulin/insulin was reduced in the *Eipr1* KO, but the reduction was also not significant (Figure 1E). These results suggest that proinsulin processing and secretion are not strongly affected by the absence of EIPR1.

We next examined the levels of other known DCV cargos, such as the proprotein convertase 1/3 (PC1/3) and proprotein convertase 2 (PC2). The *Eipr1* KO had reduced levels of PC1/3 but normal levels of PC2 (Figure 1F). Expression of

bioRxiv preprint doi: https://doi.org/10.1101/374488; this version posted July 23, 2018. The copyright holder for this preprint (which was not certified by peer review) is the author/funder, who has granted bioRxiv a license to display the preprint in perpetuity. It is made available under aCC-BY-NC 4.0 International license.

wild type EIPR1 in *Eipr1* KO cells rescued the PC1/3 defect. However, this decrease in PC1/3 has no obvious effect on proinsulin processing (Figure 1E). To examine whether the reduced levels of total proinsulin and PC1/3 were due to a transcription defect, we performed quantitative RT-PCR using total cDNA from WT and *Eipr1* KO cells. No difference was observed at the mRNA levels of these DCV cargos in *Eipr1* KO cells (Figure S2A), suggesting that EIPR1 plays a role at a post-transcriptional level in controlling the levels of proinsulin and PC1/3.

EIPR1 is required for the localization of mature DCV cargos

To investigate whether the defects in insulin secretion are due to a role of EIPR1 in DCV cargo sorting, we examined the subcellular localization of insulin by immunostaining. In wild type cells, insulin was detected as puncta spread throughout the cytoplasm (Figure 2A). By contrast, in *Eipr1* KO cells, insulin accumulated in a perinuclear region that partially overlapped with the *trans*-Golgi (TGN) marker TGN38 (Figure 2A,B). This phenotype was rescued in *Eipr1* KO cells that stably expressed wild type EIPR1 (Figure 2A,B). We also examined the localization of chromogranin A (CgA), a cargo of mature DCVs, and proinsulin, a cargo of immature DCVs. In wild type cells, CgA displayed a mostly punctate pattern throughout the cytosol, similar to that of insulin (Figure 3A). By contrast, *Eipr1* KO cells showed accumulation of CgA in the perinuclear region around the TGN (Figure 3A). Proinsulin was localized in a similar perinuclear region in both wild type and *Eipr1* KO cells (Figure 3B). These data suggest that EIPR1 affects the distribution of mature DCV cargos in insulin-secreting cells. The reduction in the levels of DCV

bioRxiv preprint doi: https://doi.org/10.1101/374488; this version posted July 23, 2018. The copyright holder for this preprint (which was not certified by peer review) is the author/funder, who has granted bioRxiv a license to display the preprint in perpetuity. It is made available under aCC-BY-NC 4.0 International license.

cargo in the cell periphery might explain the reduction in insulin secretion in *Eipr1* KO cells under stimulating conditions (Figure 1B, right panel).

To investigate whether the mature DCV cargo is stuck at the TGN in *Eipr1* KO cells, we used a pulse-chase method to monitor cargo exit from the TGN. We transiently transfected the DCV cargo ANF::GFP into WT and *Eipr1* KO 832/13 cells and blocked cargo exit from the Golgi by incubating for 2 hours at 20° (Kögel et al., 2013). We first verified that at steady state (before the temperature block), ANF::GFP accumulated in a perinuclear region in *Eipr1* KO cells (Figure S3A), similar to insulin and CgA. After the temperature block (pulse), cells were returned to 37° and incubated for different times (chase) (Figure S3B). They were then processed for GFP immunostaining and imaging. Cells were scored based on whether ANF::GFP was (1) predominantly at the TGN-region ("Golgi-like" in Figure S3C), (2) found both at the TGN-region and at the cell periphery ("Intermediate" in Figure S3C), or (3) excluded from the Golgi ("Periphery" in Figure S3C). We observed that the accumulation of ANF::GFP at the TGN was significantly different between WT and *Eipr1* KO cells at all time points (Figure S3D), confirming that EIPR1 affects the distribution of DCV cargo. The accumulation of ANF::GFP significantly changed in *Eipr1* KO cells during the chase period, with most of the cells having ANF::GFP at the Golgi at t = 0, and most of the cells having ANF::GFP at both the TGN and the periphery at t = 80 min (Figure S3D). This indicates that the DCV cargo is not permanently stuck at the TGN region in *Eipr1* KO cells but is able to reach the cell periphery, although probably at a slower rate than in WT cells.

bioRxiv preprint doi: https://doi.org/10.1101/374488; this version posted July 23, 2018. The copyright holder for this preprint (which was not certified by peer review) is the author/funder, who has granted bioRxiv a license to display the preprint in perpetuity. It is made available under aCC-BY-NC 4.0 International license.

EIPR1 is needed for the localization of EARP subunits and their association with membranes

It was recently shown that mammalian EIPR1 interacts with the EARP and GARP complex subunits and functions with EARP in endosomal recycling and with GARP in endosome-Golgi retrograde trafficking (Topalidou et al., 2016; Gershlick et al., 2016). However, *eipr-1* mutants in *C. elegans* have behavioral and cellular phenotypes similar to EARP-specific mutants, but not GARP-specific mutants (Topalidou et al., 2016). EIPR1 is a WD40 domain protein, and WD40 domains often act as scaffolds for mediating protein interactions and multi-protein complex assembly (Stirnimann et al., 2010). To investigate whether EIPR1 is required for the localization of EARP or GARP complex subunits in insulin-secreting cells, we examined the localization of transiently transfected Myc-tagged VPS50 (the sole EARP-specific subunit), GFP and Myc-tagged VPS54 (the sole GARP-specific subunit), and Myc-tagged VPS51 and VPS53 (subunits present in both the GARP and EARP complexes). We also examined the localization of endogenous VPS50 using a commercial antibody, the only antibody we have for EARP or GARP subunits that is suitable for immunofluorescence. In wild type cells, VPS50, VPS51, VPS53, and VPS54 all showed a punctate pattern of localization. The GARP-specific VPS54 subunit was localized mostly to a perinuclear region overlapping TGN38, but the other subunits were more dispersed (Figure 4A-D, S4A-C). Interestingly, the punctate localization of the EARP-specific subunit VPS50 and the EARP/GARP common subunits VPS51 and VPS53 was disrupted in *Eipr1* KO cells with fluorescence being diffuse throughout the cytoplasm (Figure 4A, C-D, S4A-B). By

bioRxiv preprint doi: https://doi.org/10.1101/374488; this version posted July 23, 2018. The copyright holder for this preprint (which was not certified by peer review) is the author/funder, who has granted bioRxiv a license to display the preprint in perpetuity. It is made available under aCC-BY-NC 4.0 International license.

contrast, the GARP-specific subunit VPS54 was still punctate and localized near the TGN in *Eipr1* KO cells (Figure 4B and S4C), and could not be distinguished from wild type in blind experiments. We conclude that EIPR1 is needed for the localization of the EARP complex subunits, but not GARP complex subunits.

To test whether the diffuse localization of EARP subunits in the *Eipr1* KO is due to a reduced association of EARP with membranes, we fractionated 832/13 cell lysates and probed for VPS50. VPS50 was found primarily in the membrane fraction (P100) in wild-type cells, but the association of VPS50 with membranes was partially lost in *Eipr1* KO cells (Figure 4E). Similarly, VPS51 was found in the membrane fraction in wild-type cells and this association was reduced in the *Eipr1* KO (Figure 4F). By contrast, the association of the GARP-specific subunit VPS54 with membranes was not altered in *Eipr1* KO cells (Figure 4G). We conclude that EIPR1 is partially required for the proper association of EARP with membranes, but is not required for membrane-association of GARP.

EIPR1 is not required for the physical interactions between EARP complex subunits

Because EIPR1 is needed for the proper localization of EARP complex subunits and WD40 domain proteins often serve as scaffolds for complex assembly, we examined whether EIPR1 is needed for the formation of the EARP complex. We first compared the levels of endogenous VPS50 and VPS51 in wild type and *Eipr1* KO 832/13 cells. *Eipr1* KO cells had reduced levels of VPS50 and VPS51, and this defect was rescued by expression of wild type EIPR1 (Figure 5A). Thus, EIPR1 is required

bioRxiv preprint doi: https://doi.org/10.1101/374488; this version posted July 23, 2018. The copyright holder for this preprint (which was not certified by peer review) is the author/funder, who has granted bioRxiv a license to display the preprint in perpetuity. It is made available under aCC-BY-NC 4.0 International license.

for expression or stability of the individual EARP subunits. To test whether these reduced protein levels were due to reduced transcription, we examined the levels of the VPS50 and VPS51 mRNAs in WT and *Eipr1* KO cells. Quantitative PCR using total cDNA from WT and *Eipr1* KO cells showed no difference in the mRNA levels of these EARP complex subunits (Figure S2B). Thus, the EARP protein subunits are less stable in the absence of EIPR1.

To determine whether EIPR1 is required for physical interactions between the individual EARP subunits, we expressed GFP-tagged VPS50 with Myc-tagged VPS51 or Myc-tagged VPS53 in wild type and *Eipr1* KO 832/13 cells and performed coimmunoprecipitation experiments. GFP-tagged VPS50 coimmunoprecipitated with either Myc-tagged VPS51 or Myc-tagged VPS53, and these interactions were not disrupted by loss of EIPR1 (Figure 5B,C). To test whether EIPR1 is required for the interactions between GARP complex subunits, we expressed GFP-tagged VPS54 with Myc-tagged VPS51 in wild type and *Eipr1* KO 832/13 cells. GFP-tagged VPS54 coimmunoprecipitated with Myc-tagged VPS51 as expected, and this interaction was not changed in *Eipr1* KO cells (Figure 5D). These data indicate that EIPR1 is not required for interactions between the individual subunits of the EARP or GARP complexes, suggesting that EIPR1 is not required for the formation of these complexes, at least under these conditions where some subunits are overexpressed.

Finally, to further examine whether the EARP complex is disrupted in the absence of EIPR1, we subjected cell lysates from wild type and *Eipr1* KO 832/13 cells to velocity sedimentation through an 8%-30% linear sucrose gradient and blotted for VPS50. VPS50 sedimented in a broad peak between the 158 and 670 kDa

bioRxiv preprint doi: https://doi.org/10.1101/374488; this version posted July 23, 2018. The copyright holder for this preprint (which was not certified by peer review) is the author/funder, who has granted bioRxiv a license to display the preprint in perpetuity. It is made available under aCC-BY-NC 4.0 International license.

standards, indicating that the protein is part of a complex (Figure 5E). Interestingly, EIPR1 sedimentation from the same cell lysate showed a similar peak to VPS50, suggesting that EIPR1 and VPS50 might be part of the same complex (Figure 5E). However, sedimentation of VPS50 was not affected by loss of EIPR1 (Figure 5F), suggesting that the EARP complex still forms in the absence of EIPR1.

EIPR1 is required for EARP function but not GARP function

EARP is required for the recycling of cargos from recycling endosomes back to the plasma membrane (Schindler et al., 2015). EIPR1 was also shown to be required for the endocytic recycling of transferrin in HAP1 cells (Gershlick et al., 2016). We examined whether EIPR1 is also required for the recycling of transferrin in 832/13 cells. Cells were incubated with Alexa 488-labeled transferrin, washed, and then chased for different times. We found that *Eipr1* KO 832/13 cells retained more transferrin than WT cells (Figure 6A), supporting the results seen in HAP1 cells (Gershlick et al., 2016). These data suggest that EIPR1 plays a role in endocytic recycling in multiple cell types.

Depletion of GARP leads to redistribution of TGN38 to cytoplasmic vesicles thought to correspond to retrograde transport intermediates (Pérez-Victoria et al., 2008). We too found that siRNA knockdown of the VPS51 subunit of the GARP complex causes redistribution of TGN38 to cytoplasmic puncta (Figure S5), but the *Eipr1* KO had no obvious change in the distribution of TGN38 (Figure 2A and S5). Thus, EIPR1 is required for both the localization and function of EARP, but is not

bioRxiv preprint doi: https://doi.org/10.1101/374488; this version posted July 23, 2018. The copyright holder for this preprint (which was not certified by peer review) is the author/funder, who has granted bioRxiv a license to display the preprint in perpetuity. It is made available under aCC-BY-NC 4.0 International license.

required for the localization of GARP or the function of GARP in the retrograde trafficking of TGN38.

The EARP complex localizes to two distinct compartments

To determine whether EARP functions at distinct cellular sites to mediate endocytic recycling and DCV cargo sorting, we examined colocalization of the EARP subunit VPS50 with CCCP1 and transferrin. CCCP1 is a coiled-coil protein that functions in DCV biogenesis and is localized near immature DCVs and the TGN (Ailion et al., 2014; Cattin-Ortolá et al., 2017), whereas transferrin is found at early and recycling endosomes. We observed that endogenous VPS50 was found at two distinct sites. At one site, VPS50 colocalized with CCCP1::GFP and at the other VPS50 colocalized with transferrin (Figure 6B). This suggests that VPS50 localizes to two distinct compartments that are related to its functions: an endocytic recycling compartment and a compartment important for DCV biogenesis.

bioRxiv preprint doi: https://doi.org/10.1101/374488; this version posted July 23, 2018. The copyright holder for this preprint (which was not certified by peer review) is the author/funder, who has granted bioRxiv a license to display the preprint in perpetuity. It is made available under aCC-BY-NC 4.0 International license.

Discussion

In this study, we demonstrate that the EARP complex interacting-protein EIPR1 regulates proper insulin secretion and distribution of mature DCV cargo. Our data indicate that cells lacking EIPR1 are capable of stimulated insulin secretion but secrete less insulin and retain it at the TGN, supporting a role for EIPR1 in the sorting of DCV cargos. We further show that EIPR1 is required for localization of EARP, but not GARP, and that EIPR1 functions similarly to EARP to control endocytic recycling and DCV cargo sorting. Consistent with its dual function, we find that the EARP complex localizes to two distinct compartments: a TGN/iDCV-related compartment and an endocytic-recycling compartment.

EIPR1 regulates DCV cargo levels and distribution

Our studies in *C. elegans* support a role for EIPR1 and EARP in sorting cargo to DCVs. *C. elegans* mutants in *eipr-1* and the EARP complex subunits have reduced levels of cargo in mature DCVs and secrete less cargo (Paquin et al., 2016; Topalidou et al., 2016). Because these studies were based on the overexpression of exogenous DCV cargos, here we investigated the role of EIPR1 in the localization and secretion of endogenous DCV cargo using the insulin-secreting 832/13 cell line. We found that cells lacking EIPR1 remain responsive to stimulated secretion, but secrete less insulin under both resting and stimulated conditions, suggesting that the DCVs carry less cargo and that neurons and endocrine cells share a conserved pathway for DCV biogenesis.

bioRxiv preprint doi: https://doi.org/10.1101/374488; this version posted July 23, 2018. The copyright holder for this preprint (which was not certified by peer review) is the author/funder, who has granted bioRxiv a license to display the preprint in perpetuity. It is made available under aCC-BY-NC 4.0 International license.

In the absence of EIPR1, mature DCV cargos accumulate at or near the Golgi. Consistent with reduced insulin secretion in *Eipr1* KO cells, we found less insulin in cytoplasmic puncta and accumulation of insulin in the TGN region. Similarly, we observed that chromogranin A accumulates in the region around the TGN in the *Eipr1* KO. Our data support a model in which the role of EIPR1 is to ensure that DCV cargos are properly sorted to the mature DCVs.

Proinsulin cleavage into mature insulin requires the prohormone convertases 1/3 and 2 (PC1/3 and PC2). Our data show that the total levels of proprotein convertase 1/3 (PC1/3) are reduced in the absence of *Eipr1* but that PC2 is not affected. If the reduction of PC1/3 led to a defect in the processing of proinsulin, we would expect an increase in proinsulin content in *Eipr1* KO. By contrast, total proinsulin levels in *Eipr1* KO were moderately reduced, but the localization of proinsulin was not changed. These results suggest that EIPR1 does not affect proinsulin processing.

EIPR1 regulates the localization of the EARP complex and its association with membranes

The WD40 domain protein EIPR1 was identified as an interactor of the EARP and GARP complexes in rat insulin-secreting cells and human neuroglioma cells (Topalidou et al., 2016; Gershlick et al., 2016). Additionally, two mass spectrometry interactome data sets found that EIPR1 interacts with EARP subunits in human HEK293T or HeLa cells (Hein et al., 2015; Huttlin et al., 2015). VPS50 was shown to pull down VPS51, VPS52, VPS53 and EIPR1, but not VPS54, as a stoichiometric

bioRxiv preprint doi: https://doi.org/10.1101/374488; this version posted July 23, 2018. The copyright holder for this preprint (which was not certified by peer review) is the author/funder, who has granted bioRxiv a license to display the preprint in perpetuity. It is made available under aCC-BY-NC 4.0 International license.

complex (Hein et al., 2015), indicating that EIPR1 may form a stable complex with EARP. Although WD40 domain proteins often act as scaffolds for the assembly of large protein complexes (Stirnimann et al., 2010), our data suggest that EIPR1 is not needed for the formation of the EARP or GARP complex. First, EIPR1 is not required for interactions between individual subunits of the EARP and GARP complexes, as shown by coimmunoprecipitation experiments. Second, sedimentation of VPS50 was not affected by loss of EIPR1, suggesting that the EARP complex still forms in the absence of EIPR1. By contrast, we find that EIPR1 is needed for the stability of the individual EARP subunits, the localization of the EARP complex subunits, and association of EARP with membranes, supporting the model that EIPR1 recruits the EARP complex to its site of action and stabilizes it there.

Although localization of the EARP subunits was disrupted in the absence of EIPR1, localization of the GARP-specific VPS54 subunit was not affected. A recent study showed that VPS54::GFP stably expressed in H4 cells is localized at the TGN region in both wild type and EIPR1 knockdown (KD) cells, but FRAP analysis showed that EIPR1 contributes to efficient GARP recruitment to the TGN (Gershlick et al., 2016). Although we found that EIPR1 is not required for GARP localization in insulinoma cells, it is possible that EIPR1 is important for the recruitment of GARP in other cell types or under different experimental conditions.

EIPR1 participates in EARP-specific functions

EARP and EIPR1 were recently shown to participate in the endocytic recycling of transferrin (Schindler et al., 2015; Gershlick et al., 2016). We also found

bioRxiv preprint doi: https://doi.org/10.1101/374488; this version posted July 23, 2018. The copyright holder for this preprint (which was not certified by peer review) is the author/funder, who has granted bioRxiv a license to display the preprint in perpetuity. It is made available under aCC-BY-NC 4.0 International license.

that EIPR1 is needed for endocytic recycling of transferrin in insulinoma cells. To test whether EIPR1 might also function with GARP, we examined the distribution of TGN38 in *Eipr1* KO and *Vps51* KD cells. In the absence of GARP, TGN38 is redistributed to cytoplasmic vesicles (Pérez-Victoria et al., 2008), but loss of EIPR1 had no obvious effect on the distribution of TGN38. Additionally, *C. elegans* GARP mutants were shown to have enlarged lysosomes in coelomocytes, but *eipr-1* and *vps-50* mutants do not have enlarged lysosomes (Topalidou et al., 2016). These results suggest that EIPR1 does not participate in GARP-specific functions, which agrees with the model that EIPR1 is required for the localization of EARP but not GARP. However, EIPR1 was reported to be required for the retrograde traffic of the Shiga toxin B subunit (STxB), whose trafficking also depends on GARP (Gershlick et al., 2016). We were unable to examine the trafficking of STxB in insulinoma 832/13 cells since we found that these cells do not take up STxB. These data together suggest that if EIPR1 functions with GARP, it is required for only a subset of GARP functions.

EARP localizes to two distinct compartments

The dual functionality of EIPR1 and EARP in endocytic recycling and DCV cargo sorting prompted us to examine the cellular distribution of EARP. We found that EARP localizes to two distinct cellular sites, one that is associated with endosomes and one associated with the TGN or immature DCVs. The endosomal recycling and DCV cargo sorting functions of EARP and EIPR1 may reflect two independent functions or may be interconnected. It is possible that the EARP

bioRxiv preprint doi: https://doi.org/10.1101/374488; this version posted July 23, 2018. The copyright holder for this preprint (which was not certified by peer review) is the author/funder, who has granted bioRxiv a license to display the preprint in perpetuity. It is made available under aCC-BY-NC 4.0 International license.

complex moves from endosomes to the Golgi to participate in the retrieval of DCV cargo or sorting factors from an endosomal compartment. Alternatively, a pool of EARP localized near the TGN and immature DCVs may function in DCV biogenesis independently of a second pool of EARP that acts to traffick cargo out of endosomes.

A connection between endosomal trafficking and DCV biogenesis?

We have demonstrated that EARP, an endosomal-recycling complex, and the EARP-interacting protein EIPR1 are involved in DCV cargo trafficking, raising the intriguing possibility that DCV biogenesis and cargo sorting at or near the TGN may require input from endosomal compartments. Several other studies have also suggested that there may be a role of endosomes in DCV biogenesis or maturation (Klumperman et al., 1998; Vo et al., 2004; Bäck et al., 2010; Edwards et al., 2009; Sumakovic et al., 2009; Topalidou et al., 2016; Zhang et al., 2017).

One possible connection of endosomes to DCV maturation is the removal of cargos from immature DCVs. The AP-1 adaptor that is involved mainly in trafficking between the trans-Golgi and endosomes has been shown to associate with immature DCVs and to mediate the removal of syntaxin 6 and mannose 6-phosphate receptors from immature DCVs (Dittie et al., 1996; Klumperman et al., 1998). Two studies on the role of *C. elegans* RAB-2 in DCV biogenesis supported the idea that RAB-2 acts at a maturation step by preventing DCV soluble cargo from getting lost through the endosomal-lysosomal system (Edwards et al., 2009; Sumakovic et al., 2009). Because *C. elegans* EIPR-1 acts in the same genetic pathway as RAB-2

bioRxiv preprint doi: https://doi.org/10.1101/374488; this version posted July 23, 2018. The copyright holder for this preprint (which was not certified by peer review) is the author/funder, who has granted bioRxiv a license to display the preprint in perpetuity. It is made available under aCC-BY-NC 4.0 International license.

(Topalidou et al., 2016), the role of EIPR-1 might also be to prevent cargo loss through the endolysosomal system.

A second possible connection of endosomes to DCV maturation is the recycling and retrieval of DCV cargos from the plasma membrane. Following DCV exocytosis, transmembrane DCV cargos may be recycled back to nascent DCVs via an endosomal pathway (Vo et al., 2004; Bäck et al., 2010). Additionally, a recent study identified a possible role for the secretory cell-specific Munc13-4 paralog BAIAP3 in this DCV recycling pathway (Zhang et al., 2017). BAIAP3 was shown to localize to late and recycling endosomes and to be needed for DCV maturation and for more general endosome recycling to the TGN (Zhang et al., 2017). Because EARP and EIPR1 act in recycling plasma membrane proteins like transferrin out of endosomes, perhaps EARP and EIPR1 are also needed for the trafficking of recycled DCV membrane cargo out of endosomes to the cellular compartments where DCVs are formed and mature. It will be interesting to determine whether DCV membrane cargos are recycled from the plasma membrane through endosomes in an EIPR1 and EARP-dependent manner.

Materials & methods

Cell culture

The 832/13 cell line is an INS-1-derived clone that was isolated by Dr. Christopher Newgard (Duke University School of Medicine) (Hohmeier et al., 2000) and obtained by Dr. Duk-Su Koh via Dr. Ian Sweet (University of Washington). Cell

bioRxiv preprint doi: https://doi.org/10.1101/374488; this version posted July 23, 2018. The copyright holder for this preprint (which was not certified by peer review) is the author/funder, who has granted bioRxiv a license to display the preprint in perpetuity. It is made available under aCC-BY-NC 4.0 International license.

lines were grown in RPMI 1640-GlutaMAX™ (GIBCO) medium supplemented with 10% FBS (RMBIO), 1 mM sodium pyruvate (GIBCO), 10 mM HEPES (GIBCO), 1X Pen/Strep (GIBCO), and 0.0005% 2-beta-mercaptoethanol at 5% CO_2 and 37°C. Cells were transfected using Lipofectamine 2000 (Thermo Fisher) according to the manufacturer's instructions.

Constructs

The plasmids VPS50::13Myc, VPS51::13Myc, VPS53::13Myc, VPS54::13Myc, VPS54::GFP, and VPS50::GFP were a gift from Juan Bonifacino (Pérez-Victoria et al., 2008; Pérez-Victoria and Bonifacino, 2009; Schindler et al., 2015).

The EIPR1_pBabe-hygro construct used for making EIPR1(+) stable lines was constructed by amplifying rat EIPR1 cDNA from an 832/13 cDNA library using primers:

oET513: 5'- ccatggatccatggaagacgacgccccg-3' and

oET514: 5'- ctgagaattctcagagcagtatgtggtacttcagtgc-3'

The PCR product was digested by EcoRI/BamHI and cloned into EcoRI/BamHI-digested pBabe-hygro (a gift from Suzanne Hoppins).

***Eipr1* knock out using CRISPR editing**

To knock out EIPR1, we performed Cas9-mediated genome editing via homology-directed repair (HDR) in 832/13 cells using the protocol described (Ran et al., 2013).

bioRxiv preprint doi: https://doi.org/10.1101/374488; this version posted July 23, 2018. The copyright holder for this preprint (which was not certified by peer review) is the author/funder, who has granted bioRxiv a license to display the preprint in perpetuity. It is made available under aCC-BY-NC 4.0 International license.

For designing guide RNAs we used the online CRISPR design tool (Ran et al., 2013) and selected three guide RNAs that recognize sequences in or near the first exon of rat *Eipr1*:

guide 1: 5'-gacgacgccccggtgatctacggg-3'

guide 2: 5'-gagcccgagtcccgcctcaccagg-3'

guide 3: 5'-gtatcatggaagacgacgccccgg-3'

The guide RNAs were cloned into pSpCas9(BB)-2A-GFP vector using the indicated protocol (Ran et al., 2013). The efficiency of the cloned guide RNAs was tested using the SURVEYOR nuclease assay (Figure S1B) according to the manufacturer's instructions (Surveyor Mutation Detection kit, Transgenomic). Guide RNA #1 was selected for all subsequent experiments.

To design the homology-directed repair (HDR) template we used the pPUR (Clontech) vector as a backbone and cloned approximately 1.5 kb *Eipr1* homology arms upstream and downstream of the puromycin selection cassette (Figure 1A and S1A). The HDR template was constructed using Gibson assembly.

To cotransfect the CRISPR plasmid (carrying Cas9 and the guide RNA) and the HDR template, cells were grown in two 10-cm petri dishes to near confluency. Cells were cotransfected with 7 μg CRISPR plasmid and 7 μg non-linearized HDR template using Lipofectamine 3000 according to the instructions (Thermo Fisher). 48 hours after transfection, the media was removed and replaced with new media together with 1 μg/ml puromycin. The puromycin selection was kept until individual clones could be picked, grown in individual dishes, and tested for CRISPR editing.

bioRxiv preprint doi: https://doi.org/10.1101/374488; this version posted July 23, 2018. The copyright holder for this preprint (which was not certified by peer review) is the author/funder, who has granted bioRxiv a license to display the preprint in perpetuity. It is made available under aCC-BY-NC 4.0 International license.

Individual puromycin-resistant clones were tested for proper CRISPR editing of the *Eipr1* gene by extracting genomic DNA and performing PCR (Figure S1C). The primers used for the PCR screening of positive clones were the following:

oET236: 5'-gaggtccgttcacccacag-3' (hybridizes just upstream of the left homology arm).

oET237: 5'-gcctggggactttccacac-3' (hybridizes in the SV40 promoter that drives the expression of the puromycin resistance gene).

5 out of 16 puromycin-resistant clones showed the band indicative of insertion of the puromycin cassette into *Eipr1*. To test for homozygosity of the insertion, we performed PCR using primers that amplify the wild-type *Eipr1* locus:

oET236: 5'-gaggtccgttcacccacag-3' (hybridizes just upstream of the left homology arm).

oET200: 5'- gagcagtatccaacacacacctc-3' (hybridizes just downstream of the Cas9 cleavage site and in the first *Eipr1* intron).

Of the 16 clones tested, three did not show the wild-type band with primers oET236 and oET200 (Figure S1C) and were subsequently tested for EIPR1 expression by Western blot. Clone #3 showed no EIPR1 expression by Western (Figure 1B) and was kept as the *Eipr1* KO line.

Insulin and proinsulin secretion

Cells were grown in 24-well plates to near confluency, washed twice with PBS, and incubated for 1 hour in 200 µl per well resting buffer (5 mM KCl, 120 mM

bioRxiv preprint doi: https://doi.org/10.1101/374488; this version posted July 23, 2018. The copyright holder for this preprint (which was not certified by peer review) is the author/funder, who has granted bioRxiv a license to display the preprint in perpetuity. It is made available under aCC-BY-NC 4.0 International license.

NaCl, 24 mM $NaHCO_3$, 1 mM $MgCl_2$, 15 mM HEPES pH 7.4). The medium was collected, cleared by centrifugation, and stored at -80˚C. The cells were incubated for 1 hour in 200 µl per well stimulating buffer (55 mM KCl, 25 mM glucose, 70 mM NaCl, 24 mM $NaHCO_3$, 1 mM $MgCl_2$, 2 mM $CaCl_2$, 15 mM HEPES pH 7.4). After stimulation, the medium was cleared by centrifugation and stored at -80°C. The cells were washed once with PBS, harvested in PBS, and extracted in 100 µl per well acid-ethanol solution (absolute ethanol:H_20:HCl, 150:47:3). The pH of the acid-ethanol solution was neutralized by addition of 20 µl of 1M Tris Base per 100 µl of acid ethanol and the samples were stored at -80°C.

Samples were assayed for insulin or proinsulin content using ELISA according to the instructions of the manufacturers (Rat/Mouse insulin ELISA, Millipore, #EZRMI-13K. Rat/Mouse proinsulin ELISA, Mercodia, #10-1232-01). Secreted insulin and proinsulin levels were normalized against total cellular protein concentration and were presented as fraction of the wild type under stimulating conditions (Fig 1C,D left panels). These values were then normalized against total cellular insulin or proinsulin levels (Fig 1C,D middle panels) to give the secretion data normalized against total insulin or proinsulin content (Fig 1C,D right panels).

ANF-GFP pulse-chase

To monitor the exit of DCV cargo from the TGN, we used a protocol similar to the one described (Kögel et al., 2013). WT and *Eipr1* KO 832/13 cells were seeded on glass coverslips and grown for 24 hours. We then transfected 100 ng of ANF::GFP (Hummer et al., 2017) with Lipofectamine 2000 for 12-16 hours at 37°C in complete

bioRxiv preprint doi: https://doi.org/10.1101/374488; this version posted July 23, 2018. The copyright holder for this preprint (which was not certified by peer review) is the author/funder, who has granted bioRxiv a license to display the preprint in perpetuity. It is made available under aCC-BY-NC 4.0 International license.

growth medium. Cells were then incubated at 20°C in PBS for 2 h in a conventional incubator (pulse) to block the formation of DCVs. 30 minutes before the end of the low temperature block, 10 μg/ml of cyclohexamide was added to the PBS to block the synthesis of new ANF::GFP. The PBS was then exchanged for growth medium and the cells were shifted to 37°C (chase) for the indicated times and then were fixed with 4% paraformaldehyde (PFA), stained, and imaged as described (see immunostaining section). Cells were scored in three categories: those that had most of the ANF::GFP concentrated at the TGN ("Golgi-like"), those that had ANF::GFP both at the TGN-region and at the cell periphery ("Intermediate"), and those where the ANF::GFP was excluded from the TGN ("Periphery"). 50 to 100 cells per time point were counted for each genotype. The experimenter was blind to the genotypes of the cell lines used and the time point. The experiment was repeated three times with similar results.

Lentiviral production, infection of cells, and selection of stable lines

Platinum-E (PlatE) retroviral packaging cells (a gift from Suzanne Hoppins) were grown for a couple of generations in DMEM-GlutaMAX™ (GIBCO) medium supplemented with 10% FBS (RMBIO), 1X Pen/Strep (GIBCO), 1 ug/ml puromycin, and 10 ug/ml blastocidin at 5% CO_2 and 37°C. On day one, approximately 3.6 x 10^5 PlatE cells per well were plated in a six-well dish in DMEM-GlutaMAX™ medium supplemented with 10% FBS and 1X Pen/Strep. On day two, a mix of 152 ul Opti-MEM (Thermo Fisher), 3 ug EIPR1_pBabe-hygro DNA, and 9 ul Fugene HD transfection reagent (Promega) was incubated for 10 minutes at room temperature

bioRxiv preprint doi: https://doi.org/10.1101/374488; this version posted July 23, 2018. The copyright holder for this preprint (which was not certified by peer review) is the author/funder, who has granted bioRxiv a license to display the preprint in perpetuity. It is made available under aCC-BY-NC 4.0 International license.

and transfected into each well. On day three, the media was removed and replaced with new PlatE media. On day four, approximately 1.5 x 10^5 *Eipr1* KO 832/13 cells per well were plated in a six-well dish in RPMI 1640-GlutaMAX, supplemented with 10% FBS, 1 mM sodium pyruvate, 10 mM HEPES, 1X Pen/Strep, and 0.0005% 2-beta-mercaptoethanol. 3 ul of 8 mg/ml hexadimethrine bromide (Sigma) was added to each well. The supernatant of the PlatE cells (48 hours viral supernatant) was collected with a sterile syringe, passed through a 0.45 micron filter, and added to the *Eipr1* KO cells. The *Eipr1* KO cells were incubated for 5-8 hours at 5% CO_2 and 37°C, then the media was changed and replaced with new media. The cells were incubated overnight at 5% CO_2 and 37°C. On day five, the supernatant was removed from the *Eipr1* KO cells and replaced with the supernatant from the PlatE cells (72 hours viral supernatant) after passing through a 0.45 micron filter. 3 ul of 8 mg/ml hexadimethrine bromide was added in each well and the cells were incubated for 5-8 hours. The media was replaced with new RPMI 1640-GlutaMAX media. On day six, the *Eipr1* KO cells were collected, transferred to a 10-cm petri dish, and 200 ug/ml hygromycin was added. The cells were grown under hygromycin selection until individual clones could be picked and tested for EIPR1 expression.

Protein extraction and coimmunoprecipitation

The anti-GFP nanobody was expressed and purified as described (Topalidou et al., 2016). For protein extraction or coimmunoprecipitation, approximately 4 X 10^6 832/13 cells were plated onto 10-cm plates. When transfection was required,

bioRxiv preprint doi: https://doi.org/10.1101/374488; this version posted July 23, 2018. The copyright holder for this preprint (which was not certified by peer review) is the author/funder, who has granted bioRxiv a license to display the preprint in perpetuity. It is made available under aCC-BY-NC 4.0 International license.

cells were transfected 24 hours later with 15ug of the relevant plasmid (or 8 ug each if two plasmids were transfected). After 24 to 48 hours the cells were washed with cold PBS twice and harvested in lysis buffer containing 50 mM Tris, pH 7.5, 150 mM NaCl, 1% NP40 and protease inhibitor cocktail (Pierce). Lysates were transferred to microcentrifuge tubes and passed 10 times through a 20G needle followed by incubation for 30 min at 4°. Lysates were centrifuged at 20,000g for 15 min at 4°. Approximately 1/10th of the supernatant was kept as input control for subsequent immunoblot analysis. The remaining lysate was incubated with 20 µg anti-GFP nanobody bound to magnetic beads for two to four hours at 4°C. The beads were washed three times with lysis buffer and resuspended in Laemmli loading buffer. The input and immunoprecipitated samples were resolved on 8% SDS-polyacrylamide gels and blotted onto PVDF membranes.

Immunoblotting

PVDF membranes were incubated in 3% milk in TBST (50 mM Tris pH 7.4, 150 mM NaCl, 0.1% Tween 20) for 1 hour at room temperature and stained with the relevant antibodies in 3% milk in TBST overnight, followed by three 5-minute washes in TBST. For the membrane fractionation, membranes were blocked with Odyssey® Blocking Buffer (PBS, 927-10100) to reduce background signal. Antibodies were incubated in the same buffer and washed with PBST (137 mM NaCl, 2.7 mM KCl, 10mM Na_2HPO_4, 1.8mM KH_2PO_4, pH 7.4 supplemented with 0.1% Tween-20). The following primary antibodies were used: rabbit polyclonal anti-GFP (1:1000, a gift from Dr. Alexey Merz), mouse monoclonal anti-c-Myc (1:1000, Santa Cruz, sc-40), mouse monoclonal anti-beta-tubulin (1:1000, ThermoFisher, BT7R,

bioRxiv preprint doi: https://doi.org/10.1101/374488; this version posted July 23, 2018. The copyright holder for this preprint (which was not certified by peer review) is the author/funder, who has granted bioRxiv a license to display the preprint in perpetuity. It is made available under aCC-BY-NC 4.0 International license.

#MA5-16308), mouse monoclonal anti-beta-tubulin (1:1,000, DHSB, E7), rabbit polyclonal anti-PCSK1 (PC1/3) (1:1000, Sigma, #SAB1100415), rabbit polyclonal anti-TSSC1/EIPR1 (1:1000, Thermo Scientific, #PA5-22360), rabbit polyclonal anti-CCDC132/VPS50 (1:1000, Sigma, #HPA026679), rabbit polyclonal anti-VPS51 (1:1000, Atlas antibodies, #HPA061447), rabbit polyclonal PC2 (1:1000, #13/4, a gift from Sharon Tooze (Dittié and Tooze, 1995)). Membranes were stained with the relevant secondary antibodies in 3% milk in TBST, followed by three 5-minute washes in TBST. The secondary antibodies used were an Alexa Fluor 680-conjugated goat anti-mouse antibody (1:20,000, Jackson Laboratory, #115-625-166), Alexa Fluor 790-conjugated donkey anti-mouse antibody (1:20,000, Jackson Laboratory, #715-655-150), or Alexa Fluor 680-conjugated goat anti-rabbit antibody (1:20,000, Jackson Laboratory, #115-625-144). A LI-COR processor was used to develop images.

Immunostaining

Approximately 1-2 X 10^5 cells per well were plated onto cover slips (Thomas Scientific #121N79) placed in 24-well cell culture plates. Cells were transfected with Lipofectamine 2000 according to manufacturer's instruction at least 24h after seeding. After 24 to 48 hours, the cells were rinsed twice with PBS and fixed with 4% paraformaldehyde (made in PBS) for 20 minutes at room temperature. The cells were rinsed twice with PBS and permeabilized with 0.5% Triton X-100 in PBS for 5 minutes at room temperature. The cells were rinsed twice with PBS and placed in 5% milk in PBS for 1 hour at room temperature. Cells were stained with primary antibodies in 0.5% milk in PBS at room temperature for 1 hour. The following

bioRxiv preprint doi: https://doi.org/10.1101/374488; this version posted July 23, 2018. The copyright holder for this preprint (which was not certified by peer review) is the author/funder, who has granted bioRxiv a license to display the preprint in perpetuity. It is made available under aCC-BY-NC 4.0 International license.

primary antibodies were used: mouse monoclonal anti-c-Myc (1:1000, Santa Cruz, sc-40), rabbit polyclonal anti-CCDC132/VPS50 (1:50, Sigma #HPA026679), mouse monoclonal anti-GFP (1:200 to 1:350, Santa Cruz, #sc-9996), mouse monoclonal anti-insulin (1:350, Sigma, #K36AC10), mouse monoclonal anti-proinsulin (1:100, Abcam, #ab8301), rabbit polyclonal anti-TGN38 (1:350, Sigma, #T9826), mouse monoclonal anti-CgA (1:350, Santa Cruz, #sc-13090). The cells were then washed with PBS three times for 5 minutes each, and incubated with rhodamine anti-rabbit secondary antibody (1:1000, Jackson Immunoresearch #111-025-144), Alexa Fluor 488 anti-rabbit secondary antibody (1:1000, Jackson Immunoresearch, #115-545-152), Alexa Fluor 488 anti-mouse secondary antibody (1:1000, Jackson Immunoresearch, #115-545-146), and Rhodamine Ret-X anti mouse secondary antibody (1:1000, Jackson Immunoresearch #715-295-150) at room temperature for 1 hour. The cells were washed with PBS three times for 5 min each, mounted onto glass slides using Vectashield (Vector laboratories H1000) or Prolong Diamond (Life Technologies P36965) and examined by fluorescence microscopy. Images were obtained using a Nikon 80i wide-field compound microscope with a 60X oil objective (numerical aperture = 1.4) or an Olympus FLUOVIEW FV1200 confocal microscope with a 60X UPlanSApo oil objective (numerical aperture = 1.35). The acquisition software used for the Nikon was NIH elements and for the Olympus it was Fluoview v4.2. Pearson's correlation coefficients were determined using Fiji and the coloc-2 plugin by taking maximum intensity projections of z-stacks and drawing a line around each individual cell.

bioRxiv preprint doi: https://doi.org/10.1101/374488; this version posted July 23, 2018. The copyright holder for this preprint (which was not certified by peer review) is the author/funder, who has granted bioRxiv a license to display the preprint in perpetuity. It is made available under aCC-BY-NC 4.0 International license.

VPS51 knockdown by RNAi

VPS51 knockdown was performed using stealth siRNA from Life Technologies (# 10620312-353281 D10, 5'-GAUGGACAGUGAGAcGGACAUGGUG-3'). Transfection of oligonucleotides (20 nM) was done using Lipofectamine 2000 as follows: cells were seeded on cover slips placed in 24-well cell culture plates until they reached approximately 50% confluence. On days one and three, cells were transfected with 1 µl of oligonucleotides and 1 µl Lipofectamine according to the manufacturer's instructions. On day five, cells were stained with the relevant antibodies following standard immunostaining procedure.

Cofractionation on sucrose velocity gradients

WT or *Eipr1* KO 832/13 cells were grown to confluence in 15-cm tissue culture plates. Cells were washed twice with ice cold PBS, transferred into microcentrifuge tubes in PBS, and centrifuged at 500g for 10 minutes at 4°C. Cells were resuspended in lysis buffer (50 mM Tris-Cl pH 7.6, 150 mM NaCl, 1% NP-40, 1 mM EDTA, protease inhibitor cocktail from Pierce), kept on ice for 20 minutes and centrifuged at 20,000g for 10 minutes at 4°C. Continuous sucrose gradients were prepared by overlaying 8% sucrose on 30% sucrose (or 8%-25% as indicated) in 50 mM Tris-Cl pH 7.6, 150 mM NaCl, 1% NP-40, 1 mM EDTA, in a 3.5 mL ultracentrifuge tube (Beckman Coulter #349622). The tubes were sealed with parafilm, set horizontally for 2 hours at 4°C, and then vertically for 1 hour at 4°C. The clarified lysate (or sizing standards) was loaded on top of the gradient. Tubes were centrifuged at 100,000g for 16h at 4˚C in a SW50 rotor. Fractions were collected

bioRxiv preprint doi: https://doi.org/10.1101/374488; this version posted July 23, 2018. The copyright holder for this preprint (which was not certified by peer review) is the author/funder, who has granted bioRxiv a license to display the preprint in perpetuity. It is made available under aCC-BY-NC 4.0 International license.

from top to bottom and supplemented with 6X SDS sample loading buffer. EARP complex subunits were analyzed by immunoblotting using antibodies to the endogenous proteins. Sizing standards (Bio-Rad #151-1901) were analyzed by Coomassie-stained SDS-PAGE gels.

Cell fractionation

We used a method similar to the one described (Cattin-Ortolá et al., 2017). Specifically, WT 832/13 or *Eipr1* KO 832/13 cells were seeded on a 24-well cell culture plate and grown until sub-confluence. Where indicated, cells were transfected with VPS51::13Myc for 48 hours before fractionation using Lipofectamine 2000, according to the manufacturer's instructions. Cells were washed twice with ice cold PBS, transferred into microcentrifuge tubes in PBS, and centrifuged at 500g for 10 minutes at 4°C. Cells were resuspended in lysis buffer (20 mM HEPES pH 7.4, 250 mM sucrose supplemented with protease inhibitors from Pierce) and disrupted by repeated passage through a 30-gauge needle. Cell lysates were centrifuged twice at 1,000g for 10 minutes at 4°C. The post-nuclear supernatant was transferred into an ultracentrifuge tube (Beckman-Coulter #343775) and centrifuged at 100,0000g for 1h at 4°C in a TLA100 rotor. The supernatant was removed and supplemented with 6X SDS loading dye. The pellet was washed once with lysis buffer, resuspended in an equal volume of lysis buffer, and supplemented with SDS loading dye. Samples were analyzed by immunoblotting as described above.

bioRxiv preprint doi: https://doi.org/10.1101/374488; this version posted July 23, 2018. The copyright holder for this preprint (which was not certified by peer review) is the author/funder, who has granted bioRxiv a license to display the preprint in perpetuity. It is made available under aCC-BY-NC 4.0 International license.

Transferrin recycling and immunostaining assays

For the transferrin recycling assay, WT and *Eipr1* KO 832/13 cells were seeded onto 24-well plates and grown in complete media until they reached confluence. Cells were placed in warm uptake medium for a 25 minute pulse (Serum free RPMI + 1% BSA + 25 mM HEPES + 50 μg/mL Alexa 488-transferrin (Invitrogen #T13342)). Medium was then exchanged for complete RPMI medium and cells were chased for the indicated times. Cells were transferred to ice, washed twice with ice-cold PBS, and detached on ice with 10mM EDTA in PBS for 30 minutes to 1 hour with manual agitation and gentle pipetting. Detached single cells were transferred into a microcentrifuge tube and fixed at 4°C with 4% PFA (final concentration ~ 3.5%) for 10 minutes on a Nutator to avoid clumping. Fixed cells were washed with PBS and analyzed by FACS using a LSRII (BD Biosciences). Data were analyzed using FlowJo.

For transferrin immunostaining, cells were seeded onto cover slips in 24-well plates for 24 to 48 hours. Cells were then placed in warm uptake medium for a 25 minute pulse (Serum free RPMI + 1% BSA + 25 mM HEPES + 50 μg/mL Alexa 568-transferrin (Invitrogen #T23365)), washed twice with PBS, and fixed with 4% PFA as already described.

Quantitative RT-PCR

WT and *Eipr1* KO cells were grown in 10 cm plates, harvested in 1 ml of TRIzol (Invitrogen), and frozen at -80°. Total RNA was isolated following the

bioRxiv preprint doi: https://doi.org/10.1101/374488; this version posted July 23, 2018. The copyright holder for this preprint (which was not certified by peer review) is the author/funder, who has granted bioRxiv a license to display the preprint in perpetuity. It is made available under aCC-BY-NC 4.0 International license.

manufacturer's protocol and cDNA was synthesized from 1 μg RNA using the QuantiTekt Reverse Transcription kit (Qiagen) according to the manufacturer's instructions. Each 10 μl qPCR reaction contained 1 μl of cDNA and 5 μl of 2× Sybr Green Master Mix (Kappa Biosystems). Absorbance was measured over 40 cycles using a CFX Connect Real-Time System (Biorad). The cycle quantification value (Cq, cycle at which the amplification curve crosses a prescribed threshold value) for each sample was measured using the provided software and normalized to actin control. The primers used were the following:

Proinsulin 1 F: 5'-atggccctgtggatgc-3'

Proinsulin 1 R: 5'-tcagttgcagtagttctccagttg-3'

PC1/3 F: 5'-atgaagcaaagaggttggactc-3'

PC1/3 R: 5'- ttaattcttctcattcagaatgtcc-3'

Actin F: 5'-atggatgacgatatcgctgc-3'

Actin R: 5'-ctagaagcatttgcggtgc-3'

VPS50 F: 5'-atgcaaaaaatcaaatctcttatgacccgg-3'

VPS50 R: 5'-tcgtttaggtctgtctatatcatctatagc-3'

VPS51 F: 5'-atggcggccgcggcagctgtggggcctggc-3'

VPS51 R: 5'-gccgcgctcgcagatgacctcgacaacact-3'

Statistics

Data were tested for normality by a Shapiro-Wilk test. When the data did not pass the normality test, we used the Kruskal-Wallis test followed by Dunn's test to

bioRxiv preprint doi: https://doi.org/10.1101/374488; this version posted July 23, 2018. The copyright holder for this preprint (which was not certified by peer review) is the author/funder, who has granted bioRxiv a license to display the preprint in perpetuity. It is made available under aCC-BY-NC 4.0 International license.

investigate whether there was statistical significance between groups. When data passed the normality test, we used a 1-way ANOVA test with Bonferroni correction.

bioRxiv preprint doi: https://doi.org/10.1101/374488; this version posted July 23, 2018. The copyright holder for this preprint (which was not certified by peer review) is the author/funder, who has granted bioRxiv a license to display the preprint in perpetuity. It is made available under aCC-BY-NC 4.0 International license.

Acknowledgements

We thank Christopher Newgard, Ian Sweet and Duk-Su Koh for the 832/13 cell line, with the support of the UW DRC Cell Function and Analysis Core; Suzanne Hoppins for the pBabe vector, platE cells, and protocol for lentiviral production and infection; Juan Bonifacino for the EARP and GARP subunit plasmids; Cedric Asensio for the ANF::GFP plasmid; Alex Merz and Sharon Tooze for antibodies. JC was supported in part by an NIH Institutional Training Grant for Neurobiology (T32 GM007108). This work was supported by a University of Washington Diabetes Research Center Pilot and Feasibility Award (NIH grant P30 DK017047), an Ellison Medical Foundation New Scholar Award, and by NIH grants R00 MH082109 and R01 GM121481. The authors declare no competing financial interests.

bioRxiv preprint doi: https://doi.org/10.1101/374488; this version posted July 23, 2018. The copyright holder for this preprint (which was not certified by peer review) is the author/funder, who has granted bioRxiv a license to display the preprint in perpetuity. It is made available under aCC-BY-NC 4.0 International license.

References

Ailion, M., M. Hannemann, S. Dalton, A. Pappas, S. Watanabe, J. Hegermann, Q. Liu, H.-F. Han, M. Gu, M.Q. Goulding, N. Sasidharan, K. Schuske, P. Hullett, S. Eimer, and E.M. Jorgensen. 2014. Two Rab2 interactors regulate dense-core vesicle maturation. *Neuron*. 82:167–180. doi:10.1016/j.neuron.2014.02.017.

Bäck, N., C. Rajagopal, R.E. Mains, and B.A. Eipper. 2010. Secretory granule membrane protein recycles through multivesicular bodies. *Traffic* 11:972–986. doi:10.1111/j.1600-0854.2010.01066.x.

Cattin-Ortolá, J., I. Topalidou, A. Dosey, A.J. Merz, and M. Ailion. 2017. The dense-core vesicle maturation protein CCCP-1 binds RAB-2 and membranes through its C-terminal domain. *Traffic*. 18:720–732. doi:10.1111/tra.12507.

Conibear, E., J.N. Cleck, and T.H. Stevens. 2003. Vps51p mediates the association of the GARP (Vps52/53/54) complex with the late Golgi t-SNARE Tlg1p. *Mol. Biol. Cell*. 14:1610–1623. doi:10.1091/mbc.E02-10-0654.

Conibear, E., and T.H. Stevens. 2000. Vps52p, Vps53p, and Vps54p form a novel multisubunit complex required for protein sorting at the yeast late Golgi. *Mol. Biol. Cell*. 11:305–323.

Dittie, A.S., N. Hajibagheri, and S.A. Tooze. 1996. The AP-1 adaptor complex binds to immature secretory granules from PC12 cells, and is regulated by ADP-ribosylation factor. *J. Cell Biol.* 132:523–536.

Dittié, A.S., and S.A. Tooze. 1995. Characterization of the endopeptidase PC2 activity towards secretogranin II in stably transfected PC12 cells. *Biochem. J.* 310:777–787.

Edwards, S.L., N.K. Charlie, J.E. Richmond, J. Hegermann, S. Eimer, and K.G. Miller. 2009. Impaired dense core vesicle maturation in Caenorhabditis elegans mutants lacking Rab2. *J. Cell Biol.* 186:881–895. doi:10.1083/jcb.200902095.

Gershlick, D.C., C. Schindler, Y. Chen, and J.S. Bonifacino. 2016. TSSC1 is novel component of the endosomal retrieval machinery. *Mol. Biol. Cell*. 27:2867–2878. doi:10.1091/mbc.E16-04-0209.

Gillingham, A.K., R. Sinka, I.L. Torres, K.S. Lilley, and S. Munro. 2014. Toward a comprehensive map of the effectors of rab GTPases. *Dev. Cell*. 31:358–373. doi:10.1016/j.devcel.2014.10.007.

Gondré-Lewis, M.C., J.J. Park, and Y.P. Loh. 2012. Cellular mechanisms for the biogenesis and transport of synaptic and dense-core vesicles. *Int. Rev. Cell Mol. Biol.* 299:27–115. doi:10.1016/B978-0-12-394310-1.00002-3.

bioRxiv preprint doi: https://doi.org/10.1101/374488; this version posted July 23, 2018. The copyright holder for this preprint (which was not certified by peer review) is the author/funder, who has granted bioRxiv a license to display the preprint in perpetuity. It is made available under aCC-BY-NC 4.0 International license.

Hannemann, M., N. Sasidharan, J. Hegermann, L.M. Kutscher, S. Koenig, and S. Eimer. 2012. TBC-8, a putative RAB-2 GAP, regulates dense core vesicle maturation in Caenorhabditis elegans. *PLoS Genet.* 8:e1002722. doi:10.1371/journal.pgen.1002722.

Hein, M.Y., N.C. Hubner, I. Poser, J. Cox, N. Nagaraj, Y. Toyoda, I.A. Gak, I. Weisswange, J. Mansfeld, F. Buchholz, A.A. Hyman, and M. Mann. 2015. A human interactome in three quantitative dimensions organized by stoichiometries and abundances. *Cell*. 163:712–723. doi:10.1016/j.cell.2015.09.053.

Hohmeier, H.E., H. Mulder, G. Chen, R. Henkel-Rieger, M. Prentki, and C.B. Newgard. 2000. Isolation of INS-1-derived cell lines with robust ATP-sensitive K+ channel-dependent and -independent glucose-stimulated insulin secretion. *Diabetes*. 49:424–430. doi:10.2337/diabetes.49.3.424.

Hummer, B.H., N.F. de Leeuw, C. Burns, L. Chen, M.S. Joens, B. Hosford, J.A.J. Fitzpatrick, and C.S. Asensio. 2017. HID-1 controls formation of large dense core vesicles by influencing cargo sorting and trans-Golgi network acidification. *Mol. Biol. Cell*. 28:3870–3880. doi:10.1091/mbc.E17-08-0491.

Huttlin, E.L., L. Ting, R.J. Bruckner, F. Gebreab, M.P. Gygi, J. Szpyt, S. Tam, G. Zarraga, G. Colby, K. Baltier, R. Dong, V. Guarani, L.P. Vaites, A. Ordureau, R. Rad, B.K. Erickson, M. Wühr, J. Chick, B. Zhai, D. Kolippakkam, J. Mintseris, R.A. Obar, T. Harris, S. Artavanis-Tsakonas, M.E. Sowa, P. De Camilli, J.A. Paulo, J.W. Harper, and S.P. Gygi. 2015. The BioPlex Network: A Systematic Exploration of the Human Interactome. *Cell*. 162:425–440. doi:10.1016/j.cell.2015.06.043.

Klumperman, J., R. Kuliawat, J.M. Griffith, H.J. Geuze, and P. Arvan. 1998. Mannose 6-phosphate receptors are sorted from immature secretory granules via adaptor protein AP-1, clathrin, and syntaxin 6-positive vesicles. *J. Cell Biol.* 141:359–371.

Kögel, T., R. Rudolf, E. Hodneland, J. Copier, R. Regazzi, S.A. Tooze, and H.-H. Gerdes. 2013. Rab3D Is Critical for Secretory Granule Maturation in PC12 Cells. *PLoS ONE*. 8:e57321. doi:10.1371/journal.pone.0057321.

Mesa, R., S. Luo, C.M. Hoover, K. Miller, A. Minniti, N. Inestrosa, and M.L. Nonet. 2011. HID-1, a New Component of the Peptidergic Signaling Pathway. *Genetics*. 187:467–483. doi:10.1534/genetics.110.121996.

Paquin, N., Y. Murata, A. Froehlich, D.T. Omura, M. Ailion, C.L. Pender, M. Constantine-Paton, and H.R. Horvitz. 2016. The Conserved VPS-50 Protein Functions in Dense-Core Vesicle Maturation and Acidification and Controls Animal Behavior. *Curr. Biol.* 26:862–871. doi:10.1016/j.cub.2016.01.049.

bioRxiv preprint doi: https://doi.org/10.1101/374488; this version posted July 23, 2018. The copyright holder for this preprint (which was not certified by peer review) is the author/funder, who has granted bioRxiv a license to display the preprint in perpetuity. It is made available under aCC-BY-NC 4.0 International license.

Pérez-Victoria, F.J., and J.S. Bonifacino. 2009. Dual roles of the mammalian GARP complex in tethering and SNARE complex assembly at the trans-golgi network. *Mol. Cell. Biol.* 29:5251–5263. doi:10.1128/MCB.00495-09.

Pérez-Victoria, F.J., G.A. Mardones, and J.S. Bonifacino. 2008. Requirement of the human GARP complex for mannose 6-phosphate-receptor-dependent sorting of cathepsin D to lysosomes. *Mol. Biol. Cell*. 19:2350–2362. doi:10.1091/mbc.e07-11-1189.

Perez-Victoria, F.J., C. Schindler, J.G. Magadan, G.A. Mardones, C. Delevoye, M. Romao, G. Raposo, and J.S. Bonifacino. 2010. Ang2/Fat-Free Is a Conserved Subunit of the Golgi-associated Retrograde Protein Complex. *Mol Biol Cell*. 21:3386–3395. doi:10.1091/mbc.E10-05-0392.

Ran, F.A., P.D. Hsu, J. Wright, V. Agarwala, D.A. Scott, and F. Zhang. 2013. Genome engineering using the CRISPR-Cas9 system. *Nat. Protoc.* 8:2281–2308. doi:10.1038/nprot.2013.143.

Schindler, C., Y. Chen, J. Pu, X. Guo, and J.S. Bonifacino. 2015. EARP is a multisubunit tethering complex involved in endocytic recycling. *Nat. Cell Biol.* 17:639–650. doi:10.1038/ncb3129.

Stirnimann, C.U., E. Petsalaki, R.B. Russell, and C.W. Müller. 2010. WD40 proteins propel cellular networks. *Trends Biochem. Sci.* 35:565–574. doi:10.1016/j.tibs.2010.04.003.

Sumakovic, M., J. Hegermann, L. Luo, S.J. Husson, K. Schwarze, C. Olendrowitz, L. Schoofs, J. Richmond, and S. Eimer. 2009. UNC-108/RAB-2 and its effector RIC-19 are involved in dense core vesicle maturation in Caenorhabditis elegans. *J. Cell Biol.* 186:897–914. doi:10.1083/jcb.200902096.

Topalidou, I., J. Cattin-Ortolá, A.L. Pappas, K. Cooper, G.E. Merrihew, M.J. MacCoss, and M. Ailion. 2016. The EARP Complex and Its Interactor EIPR-1 Are Required for Cargo Sorting to Dense-Core Vesicles. *PLOS Genet.* 12:e1006074. doi:10.1371/journal.pgen.1006074.

Vo, Y.P., J.C. Hutton, and J.K. Angleson. 2004. Recycling of the dense-core vesicle membrane protein phogrin in Min6 beta-cells. *Biochem. Biophys. Res. Commun.* 324:1004–1010. doi:10.1016/j.bbrc.2004.09.147.

Yu, Y., L. Wang, Y. Jiu, Y. Zhan, L. Liu, Z. Xia, E. Song, P. Xu, and T. Xu. 2011. HID-1 is a novel player in the regulation of neuropeptide sorting. *Biochem. J.* 434:383–390. doi:10.1042/BJ20110027.

Zhang, X., S. Jiang, K.A. Mitok, L. Li, A.D. Attie, and T.F.J. Martin. 2017. BAIAP3, a C2 domain-containing Munc13 protein, controls the fate of dense-core vesicles

bioRxiv preprint doi: https://doi.org/10.1101/374488; this version posted July 23, 2018. The copyright holder for this preprint (which was not certified by peer review) is the author/funder, who has granted bioRxiv a license to display the preprint in perpetuity. It is made available under aCC-BY-NC 4.0 International license.

in neuroendocrine cells. *J. Cell Biol.* 216:2151–2166. doi:10.1083/jcb.201702099.

bioRxiv preprint doi: https://doi.org/10.1101/374488; this version posted July 23, 2018. The copyright holder for this preprint (which was not certified by peer review) is the author/funder, who has granted bioRxiv a license to display the preprint in perpetuity. It is made available under aCC-BY-NC 4.0 International license.

Figure legends

Figure 1.

Insulin secretion is reduced in *Eipr1* KO cells

(A) Strategy used to create the *Eipr1* KO 832/13 cell line. Cas9 was targeted to cut in the first exon of the rat *Eipr1* locus and homologous recombination (HR) was used to insert a puromycin cassette.

(B) *Eipr1* KO cells do not express wild type EIPR1. Protein extracts from 832/13 (WT), *Eipr1* KO 832/13 (Eipr1KO), and *Eipr1* KO 832/13 cells expressing a wild type *Eipr1* cDNA (Eipr1(+)) were blotted with an EIPR1 antibody. β-tubulin served as a loading control.

(C)(Left panel) Insulin secretion under resting (5 mM KCl, 0 mM glucose) and stimulating conditions (55 mM KCl, 25 mM glucose) from 832/13 cells (WT), *Eipr1* KO 832/13 cells (Eipr1KO), and an *Eipr1* KO stable line expressing wild type *Eipr1* (Eipr1(+)). All values were normalized to the value of the WT under stimulating conditions. n= 7, * $p<0.05$, ** $p<0.01$, ns $p>0.05$, error bars = SEM. (Middle panel) Total insulin content in WT, *Eipr1* KO, and Eipr1(+) cells. All values were normalized to the WT. n= 5; ns $p>0.05$, error bars = SEM. (Right panel) Insulin secretion normalized to insulin content under resting (5 mM KCl, 0 mM glucose) and stimulating conditions (55 mM KCl, 25 mM glucose) from WT, *Eipr1* KO, and Eipr1(+) cells. n= 7, * $p<0.05$, ** $p<0.01$, ns $p>0.05$, error bars = SEM.

(D) (Left panel) Proinsulin secretion under resting (5 mM KCl, 0 mM glucose) and stimulating conditions (55 mM KCl, 25 mM glucose) from WT, *Eipr1* KO, and

bioRxiv preprint doi: https://doi.org/10.1101/374488; this version posted July 23, 2018. The copyright holder for this preprint (which was not certified by peer review) is the author/funder, who has granted bioRxiv a license to display the preprint in perpetuity. It is made available under aCC-BY-NC 4.0 International license.

Eipr1(+) cells. All values were normalized to the value of the WT under stimulating conditions. n= 6, error bars = SEM. (Middle panel) Total proinsulin content in WT, *Eipr1* KO, and Eipr1(+) cells. All values were normalized to the WT. n= 6, *** $p<0.001$, ns $p>0.05$, error bars = SEM. (Right panel) Proinsulin secretion normalized to proinsulin content under resting (5 mM KCl, 0 mM glucose) and stimulating conditions (55 mM KCl, 25 mM glucose) from WT, *Eipr1* KO, and Eipr1(+) cells. All values were normalized to the WT under stimulating conditions. n= 6, ns $p>0.05$, error bars = SEM.

(E) Ratio of total cellular proinsulin to total insulin. n= 4, ns $p>0.05$, error bars = SEM.

(F) Levels of processed PC1/3 are reduced in *Eipr1* KO 832/13 cells but levels of processed PC2 are unchanged. Protein extracts from 832/13 (WT), *Eipr1* KO 832/13 (Eipr1KO), and *Eipr1* KO 832/13 cells expressing wild type *Eipr1* (Eipr1(+)) were blotted with antibodies against PC1/3 and PC2. β-tubulin served as a loading control.

Figure 2. Insulin localization is disrupted in *Eipr1* KO cells

(A) Representative images of 832/13 (WT), *Eipr1* KO 832/13 (Eipr1KO), and *Eipr1* KO 832/13 cells expressing wild type *Eipr1* (Eipr1(+)) costained for endogenous insulin and TGN38. In WT and Eipr1(+) cells, insulin is spread throughout the cytoplasm, but in *Eipr1* KO cells insulin accumulates in a perinuclear region that partially overlaps with TGN38. The experiment was repeated at least three times

bioRxiv preprint doi: https://doi.org/10.1101/374488; this version posted July 23, 2018. The copyright holder for this preprint (which was not certified by peer review) is the author/funder, who has granted bioRxiv a license to display the preprint in perpetuity. It is made available under aCC-BY-NC 4.0 International license.

and the experimenter was blinded to the genotypes of the stained cells. Scale bars: 5 μm.

(B) Pearson's correlation coefficient was measured to quantify the localization between insulin and the TGN marker TGN38. n=12 for WT, n=14 for *Eipr1* KO and n=18 for Eipr1(+), ** $p<0.01$, * $p<0.05$, ns $p>0.05$, error bars = SEM. The experiment was repeated three times.

Figure 3. Localization of chromogranin A and proinsulin in *Eipr1* KO cells

(A) Representative images of 832/13 (WT) and *Eipr1* KO 832/13 (Eipr1KO) cells costained for endogenous chromogranin A (CgA) and TGN38. In WT cells, CgA is spread throughout the cytoplasm, but in *Eipr1* KO cells CgA accumulates in a perinuclear region that partially overlaps with TGN38. Scale bars: 5 μm.

(B) Representative images of 832/13 (WT) and *Eipr1* KO 832/13 (Eipr1KO) cells costained for endogenous proinsulin and TGN38. In both WT and *Eipr1* KO cells, proinsulin is localized in a perinuclear region that partially overlaps with TGN38. Scale bars: 5 μm.

Figure 4. Localization and membrane association of EARP are disrupted in *Eipr1* KO cells

(A) Representative images of 832/13 (WT) and *Eipr1* KO 832/13 (Eipr1KO) cells transfected with VPS50::13Myc (VPS50::Myc) and costained with anti-Myc and anti-TGN38 antibodies. In WT cells, VPS50::Myc is localized to puncta but in *Eipr1* KO

bioRxiv preprint doi: https://doi.org/10.1101/374488; this version posted July 23, 2018. The copyright holder for this preprint (which was not certified by peer review) is the author/funder, who has granted bioRxiv a license to display the preprint in perpetuity. It is made available under aCC-BY-NC 4.0 International license.

cells fluorescence is diffuse throughout the cytoplasm. The punctate pattern of localization of VPS50::Myc overlaps only partially with TGN38. Scale bars: 5 μm.

(B) Representative images of 832/13 cells (WT) and *Eipr1* KO 832/13 (Eipr1KO) cells transfected with VPS54::GFP and costained with anti-GFP and anti-TGN38 antibodies. In both WT and *Eipr1* KO cells, VPS54::GFP is localized to perinuclear puncta that largely overlap with TGN38. Scale bars: 5 μm.

(C) Representative images of 832/13 (WT) and *Eipr1* KO 832/13 (Eipr1KO) cells transfected with VPS51::13Myc (VPS51::Myc) and stained with anti-Myc antibody. In WT cells, VPS51:: Myc is localized to puncta, but in *Eipr1* KO cells fluorescence is diffuse throughout the cytoplasm. Scale bars: 5 μm.

(D) Representative images of 832/13 (WT) and *Eipr1* KO 832/13 (Eipr1KO) cells transfected with VPS53::13Myc (VPS53::Myc) and stained with anti-Myc antibody. In wild type cells, VPS53:: Myc is localized to puncta but in *Eipr1* KO cells fluorescence is diffuse throughout the cytoplasm. Scale bars: 5 μm.

(E) VPS50 associates with membranes in an EIPR1-dependent manner. In WT cell fractions, endogenous VPS50 was found primarily in the post-nuclear P100 membrane fraction. In *Eipr1* KO 832/13 cells (Eipr1KO), VPS50 was equally distributed between the P100 membrane fraction and the S100 cytosolic fraction. β-tubulin served as a control soluble protein. S100, P100: supernatant and pellet fractions obtained by a 100,000g spin of the cell lysate, containing cytosolic and membrane-associated proteins respectively.

(F) VPS51 associates with membranes in an EIPR1-dependent manner. In WT cell fractions, VPS51::Myc was roughly equally distributed between the post-nuclear

bioRxiv preprint doi: https://doi.org/10.1101/374488; this version posted July 23, 2018. The copyright holder for this preprint (which was not certified by peer review) is the author/funder, who has granted bioRxiv a license to display the preprint in perpetuity. It is made available under aCC-BY-NC 4.0 International license.

P100 membrane fraction and the S100 cytosolic fraction, and endogenous VPS51 was found primarily in the P100 membrane fraction. In *Eipr1* KO 832/13 cells (Eipr1KO), VPS51::Myc was found mostly in the soluble fraction and endogenous VPS51 was equally distributed between the membrane fraction and the cytosolic fraction.

(G) VPS54 associates with membranes in an EIPR1-independent manner. In both WT and *Eipr1* KO 832/13 cell fractions, VPS54::Myc was equally distributed between the post-nuclear P100 membrane fraction and the S100 cytosolic fraction.

Figure 5. EIPR1 is required for normal levels of EARP protein subunits but is not required for their physical interactions.

(A) VPS50 and VPS51 levels are reduced in *Eipr1* KO cells. Protein extracts from 832/13 (WT), *Eipr1* KO 832/13 (Eipr1KO), and *Eipr1* KO 832/13 cells expressing wild type *Eipr1* (Eipr1(+)) were blotted with antibodies against VPS50 and VPS51. β-tubulin served as a loading control.

(B) VPS50 interacts with VPS51 in an EIPR1-independent way. EGFP-tagged VPS50 was coexpressed with 13Myc-tagged VPS51 in 832/13 (WT) and *Eipr1* KO 832/13 (Eipr1KO) cells. Immunoprecipitation of VPS50::GFP pulled down VPS51::Myc independently of EIPR1, but did not pull down β-tubulin. IN: input, IP: immunoprecipitated.

(C) VPS50 interacts with VPS53 in an EIPR1-independent way. EGFP-tagged VPS50 was coexpressed with 13Myc-tagged VPS53 in 832/13 (WT) and *Eipr1* KO 832/13 (Eipr1KO) cells. Immunoprecipitation of VPS50::GFP pulled down VPS53::Myc

bioRxiv preprint doi: https://doi.org/10.1101/374488; this version posted July 23, 2018. The copyright holder for this preprint (which was not certified by peer review) is the author/funder, who has granted bioRxiv a license to display the preprint in perpetuity. It is made available under aCC-BY-NC 4.0 International license.

independently of EIPR1, but did not pull down β-tubulin. IN: input, IP: immunoprecipitated.

(D) VPS51 interacts with VPS54 in an EIPR1-independent way. EGFP-tagged VPS54 was coexpressed with 13Myc-tagged VPS51 in 832/13 (WT) and *Eipr1* KO 832/13 (Eipr1KO) cells. Immunoprecipitation of VPS54::GFP pulled down VPS51::Myc independently of EIPR1, but did not pull down β-tubulin. IN: input, IP: immunoprecipitated

(E) VPS50 and EIPR1 cofractionate on a linear 8%-30% sucrose velocity gradient. Fractions from 832/13 (WT) cell lysate were blotted with antibodies against VPS50 and EIPR1. β-tubulin served as a control soluble protein.

(F) VPS50 fractionates similarly from cell lysates of 832/13 (WT) and 832/13 *Eipr1* KO (Eipr1KO) cells on a linear 8%-25% sucrose velocity gradient. Fractions from 832/13 (WT) and 832/13 *Eipr1* KO cell lysates were blotted with antibodies against VPS50.

Figure 6. EIPR1 is needed for transferrin recycling in insulinoma cells and EARP localizes to two distinct compartments.

(A) EIPR1 is needed for transferrin (Tf) recycling. FACS analysis of Alexa 488-labeled transferrin in WT and *Eipr1* KO cells at different chase times following 25 min transferrin uptake. The plot represents the median of Alexa 488–Tf intensity of the population of cells at each time point normalized to the median intensity at t = 0 as a function of time. The experiment was repeated three times with similar results.

bioRxiv preprint doi: https://doi.org/10.1101/374488; this version posted July 23, 2018. The copyright holder for this preprint (which was not certified by peer review) is the author/funder, who has granted bioRxiv a license to display the preprint in perpetuity. It is made available under aCC-BY-NC 4.0 International license.

(B) EARP localizes to two distinct compartments: a CCCP1-positive compartment that is associated with the TGN and immature DCVs and a transferrin-positive compartment that is associated with endosomes. 832/13 cells were transiently transfected with GFP-tagged CCCP1, incubated with Alexa 568-labeled transferrin (Tf) and immunostained for VPS50 and GFP. (Left) Representative confocal images of cells costained for endogenous VPS50 and GFP. Scale bars: 5 μm. (Right) The graph shows a representative intensity plot of normalized signal intensity versus distance in μm across the red line shown in the left panel. CCCP1::GFP is shown in green, Tf-Alexa 568 is in magenta, and VPS50 in cyan). White arrowhead: overlap between VPS50 and Tf. Black arrowhead: overlap between VPS50 and CCCP1.

Figure S1. *Eipr1* KO strategy using the CRISPR technology

(A) To make the *Eipr1* KO 832/13 cell line, Cas9-induced DNA cleavage was used to insert a puromycin cassette in the first exon of *Eipr1*. oET236, oET237 and oET200 are the primers used in (C) for detecting the positive clones.

(B) Surveyor nuclease assay testing the efficiency of three different guide RNAs (1, 2, 3) and the combination of guide RNAs #1 and #2 (1+2). All three guide RNAs recognize sequences at or around the 1st exon of rat *Eipr1*. Guide RNA #1 was used for all subsequent experiments. C: control.

(C) PCR detection of the *Eipr1* CRISPR positive clones using the indicated primers. Primers oET236 and oET237 detect clones positive for the puromycin insertion. Primers oET236 and oET200 detect clones that contain the wild type product. Clones #3 and #5 were selected as candidate *Eipr1* KOs. A Western blot showed that

bioRxiv preprint doi: https://doi.org/10.1101/374488; this version posted July 23, 2018. The copyright holder for this preprint (which was not certified by peer review) is the author/funder, who has granted bioRxiv a license to display the preprint in perpetuity. It is made available under aCC-BY-NC 4.0 International license.

clone #3 lacked EIPR1 expression (Figure 1A), but that #5 still expressed the wild type EIPR1 product. Clone #3 was used for all the *Eipr1* KO experiments in this study.

Figure S2. EIPR1 knock out does not affect transcription of DCV cargos and EARP or GARP subunits.

No change in transcript abundance of (A) proinsulin and PC1/3 or (B) VPS50 and VPS51 in *Eipr1* KO cells as measured by qRT-PCR. Actin served as an internal control. The Cq mean for the target genes was normalized against the Cq mean for the actin control.

Figure S3. Monitoring the exit of ANF::GFP from the TGN using a pulse-chase method.

(A) Representative images of WT and *Eipr1* KO 832/13 cells transfected with ANF::GFP and costained with anti-GFP and anti-TGN38 antibodies. In WT cells, ANF::GFP is distributed in cytoplasmic puncta, but in *Eipr1* KO cells, ANF::GFP is restricted to perinuclear puncta. Not all cells in this field of view are transfected with ANF::GFP. Scale bars: 10 μm.

(B) Schematic of the pulse-chase experiment. Cells transiently transfected with ANF::GFP were incubated at 20°C for 2 h to cause the accumulation of DCV cargos at the TGN (pulse). 30 minutes before the end of the temperature block, cyclohexamide was added to block protein translation. At the end of the temperature block, cells

bioRxiv preprint doi: https://doi.org/10.1101/374488; this version posted July 23, 2018. The copyright holder for this preprint (which was not certified by peer review) is the author/funder, who has granted bioRxiv a license to display the preprint in perpetuity. It is made available under aCC-BY-NC 4.0 International license.

were returned to 37°C and incubated for various times (chase) before fixation and immunostaining.

(C) Representative images of the cell categories used for qualitative assessment of TGN exit: (1) ANF::GFP concentrated at the TGN region (Golgi-like), (2) ANF::GFP distributed both at the TGN and at the cell periphery (Intermediate), or (3) ANF::GFP excluded from the TGN (Periphery). Scale bar: 5 μm.

(D) Percentage of WT and *Eipr1* KO cells with the indicated ANF::GFP distribution at the indicated time points. The data from one representative experiment are plotted. For each data point and each genotype, 50 to100 cells were counted blindly. The experiment was repeated three times with similar results.

Figure S4. Localization of VPS53::Myc and endogenous VPS50 is disrupted in *Eipr1* KO cells, but VPS54::Myc is not affected

(A) Representative images of 832/13 (WT) and *Eipr1* KO 832/13 (Eipr1KO) cells transfected with VPS53::13Myc (VPS53::Myc) and costained with anti-Myc and anti-TGN38 antibodies. VPS53::Myc is punctate in WT cells, but diffuse throughout the cytoplasm in *Eipr1* KO cells. The punctate pattern of localization of VPS53::Myc does not overlap with TGN38. Scale bars: 5 μm.

(B) Representative images of 832/13 (WT) and *Eipr1* KO 832/13 (Eipr1KO) cells stained with anti-VPS50 antibody. Endogenous VPS50 is punctate in WT cells, but diffuse throughout the cytoplasm in *Eipr1* KO cells. Scale bars: 5 μm.

(C) Representative images of 832/13 (WT) and *Eipr1* KO 832/13 (Eipr1KO) cells transfected with VPS54::13Myc (VPS54::Myc) and stained with anti-Myc antibody.

bioRxiv preprint doi: https://doi.org/10.1101/374488; this version posted July 23, 2018. The copyright holder for this preprint (which was not certified by peer review) is the author/funder, who has granted bioRxiv a license to display the preprint in perpetuity. It is made available under aCC-BY-NC 4.0 International license.

VPS54::Myc is localized in a perinuclear region in both WT and *Eipr1* KO cells. Scale bars: 5 μm.

Figure S5. TGN38 is redistributed in *Vps51* knockdown but not *Eipr1* KO cells

Representative images of 832/13 cells (WT), *Vps51* siRNA knockdown 832/13 cells (Vps51KD), and *Eipr1* KO cells (Eipr1KO) stained for TGN38. TGN38 is partially redistributed to cytoplasmic puncta in VPS51 knockdown cells, but is still localized to the Golgi in *Eipr1* KO cells.

Figure 1

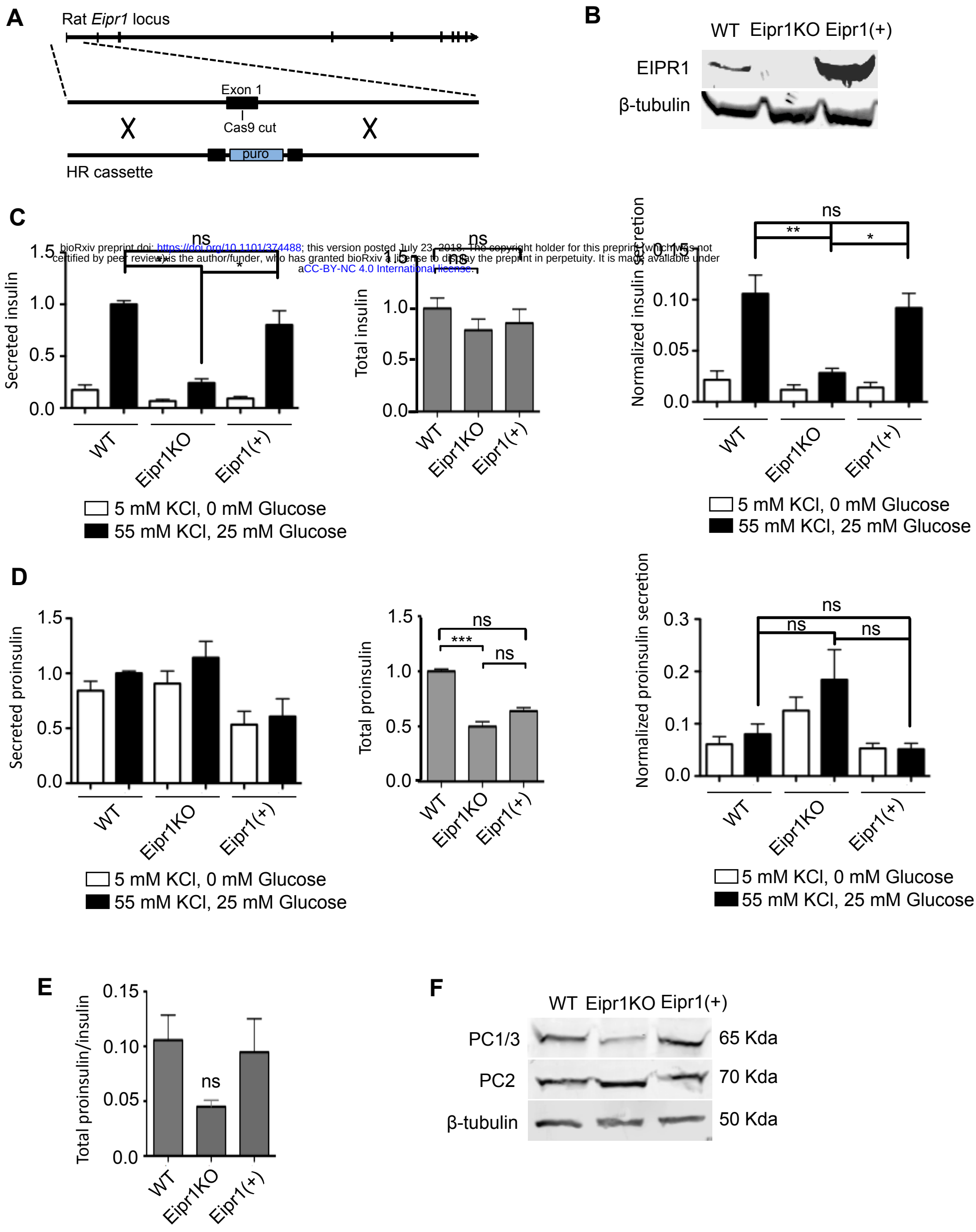

bioRxiv preprint doi: https://doi.org/10.1101/374488; this version posted July 23, 2018. The copyright holder for this preprint (which was not certified by peer review) is the author/funder, who has granted bioRxiv a license to display the preprint in perpetuity. It is made available under aCC-BY-NC 4.0 International license.

Figure 2

A

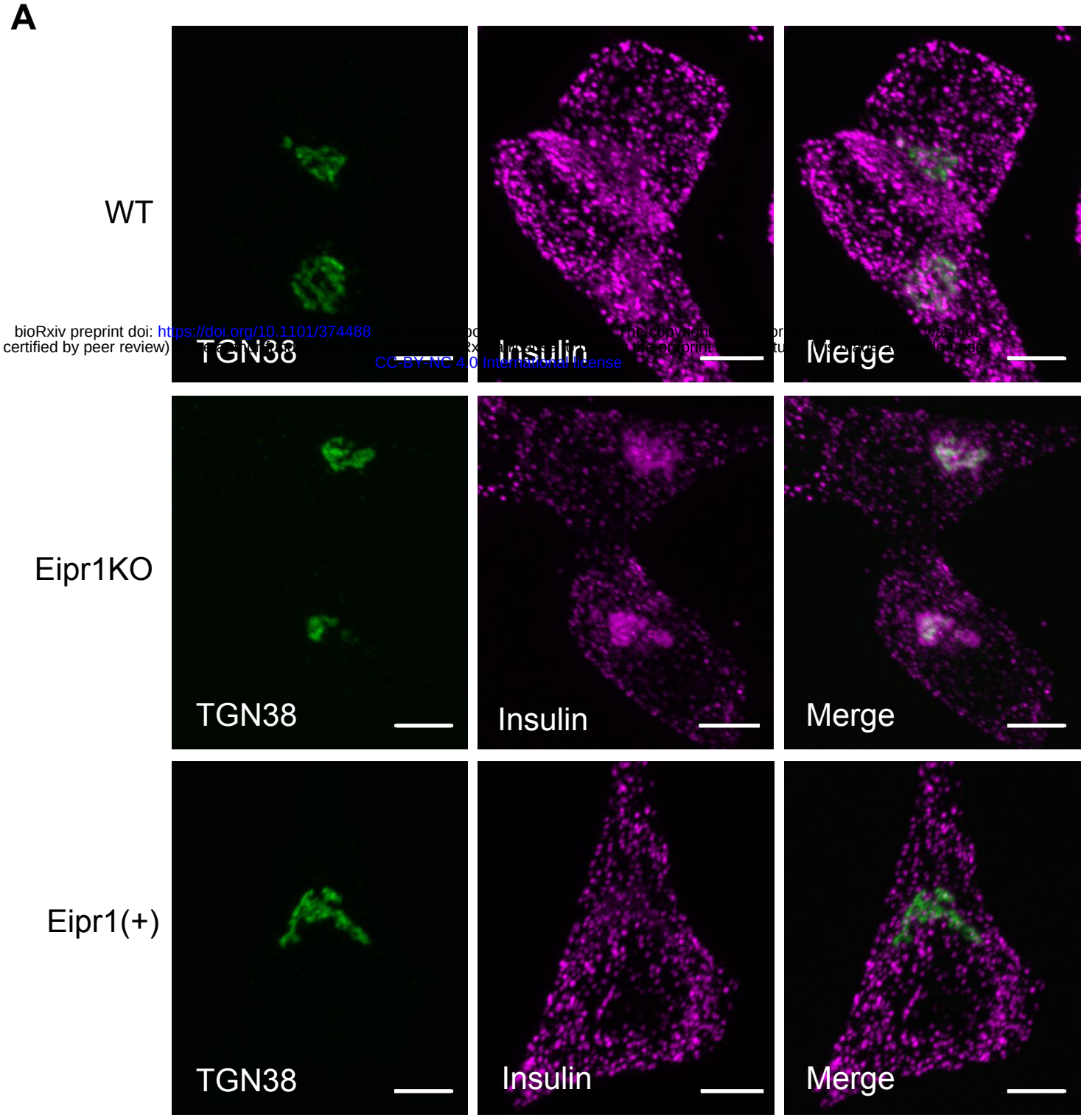

bioRxiv preprint doi: https://doi.org/10.1101/374488
certified by peer review)
CC-BY-NC 4.0 International license

B

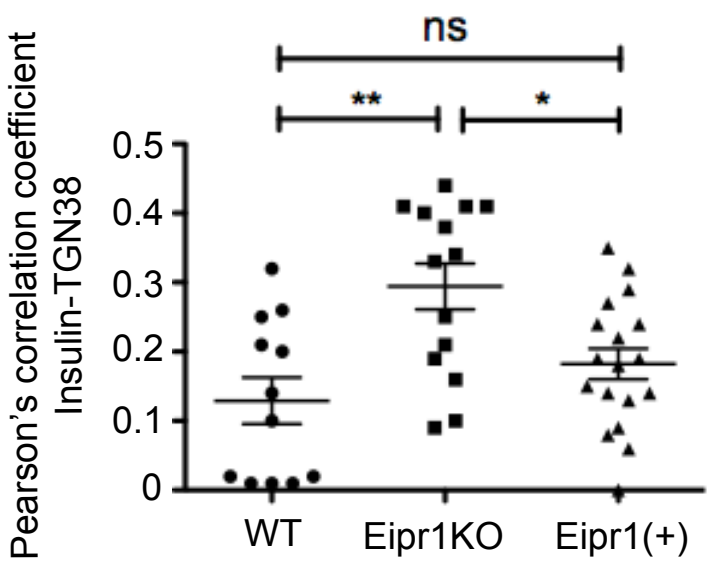

Figure 3

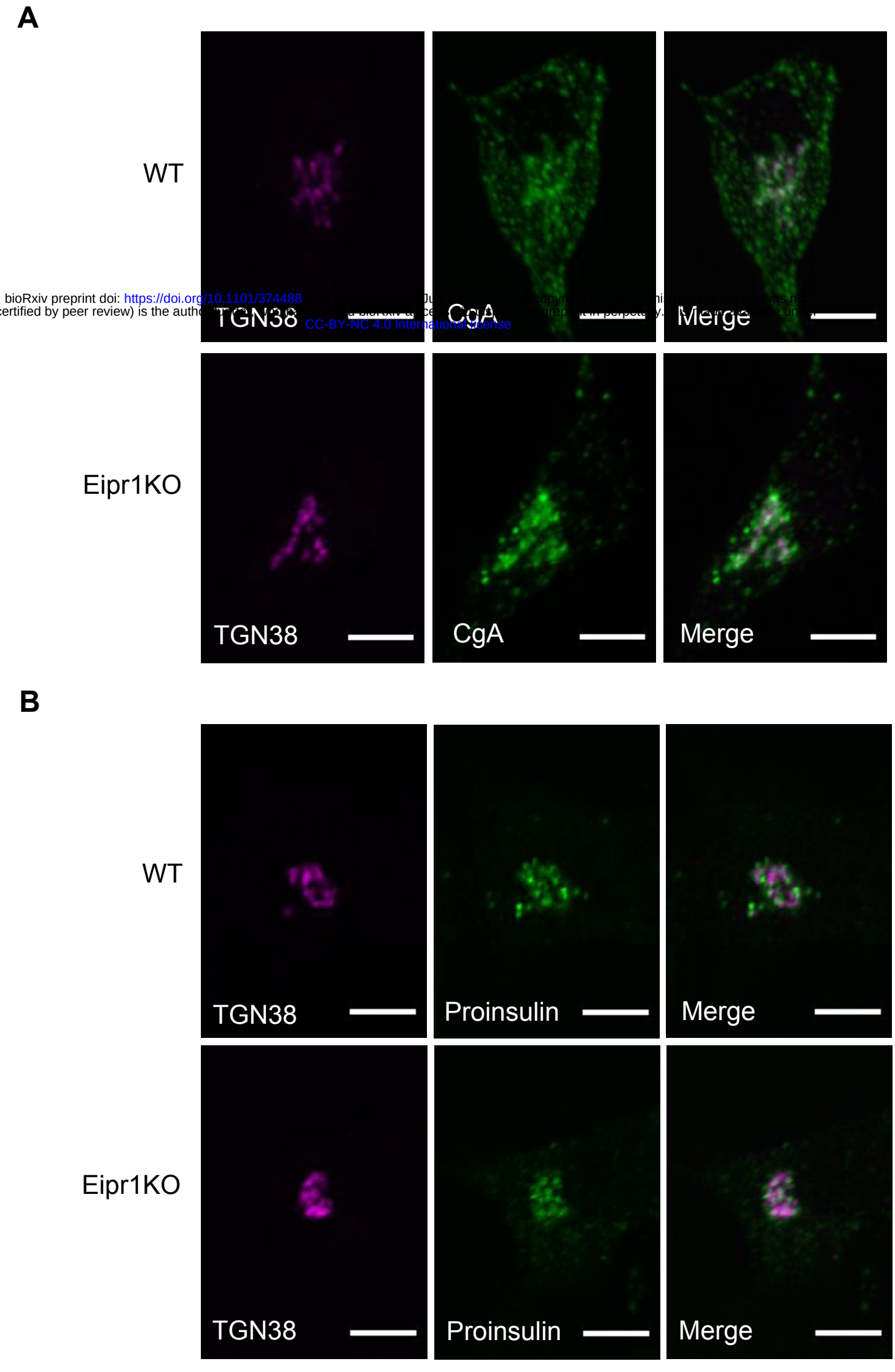

bioRxiv preprint doi: https://doi.org/10.1101/374488
certified by peer review) is the author
CC-BY-NC 4.0 International license

Figure 4

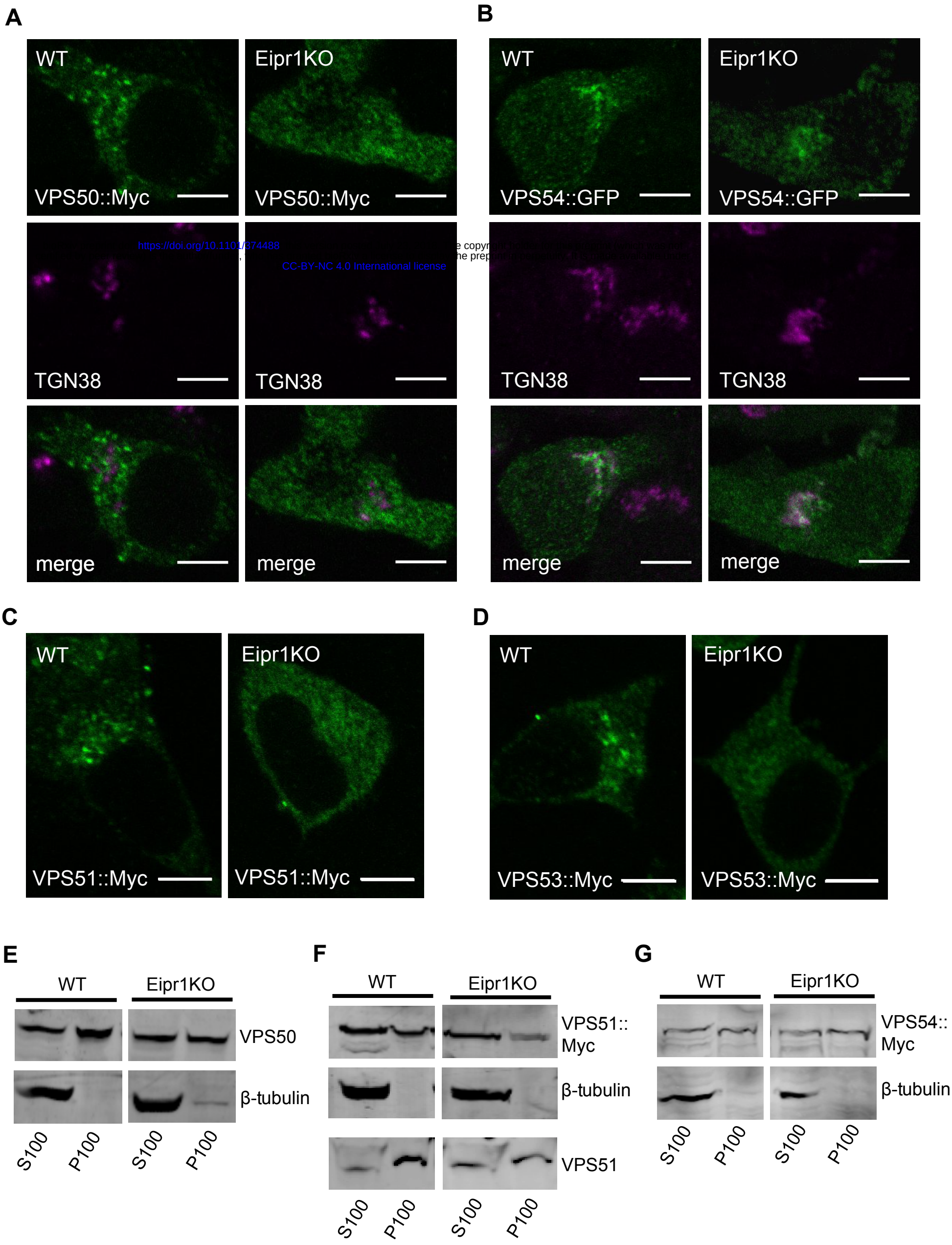

https://doi.org/10.1101/374488
CC-BY-NC 4.0 International license

Figure 5

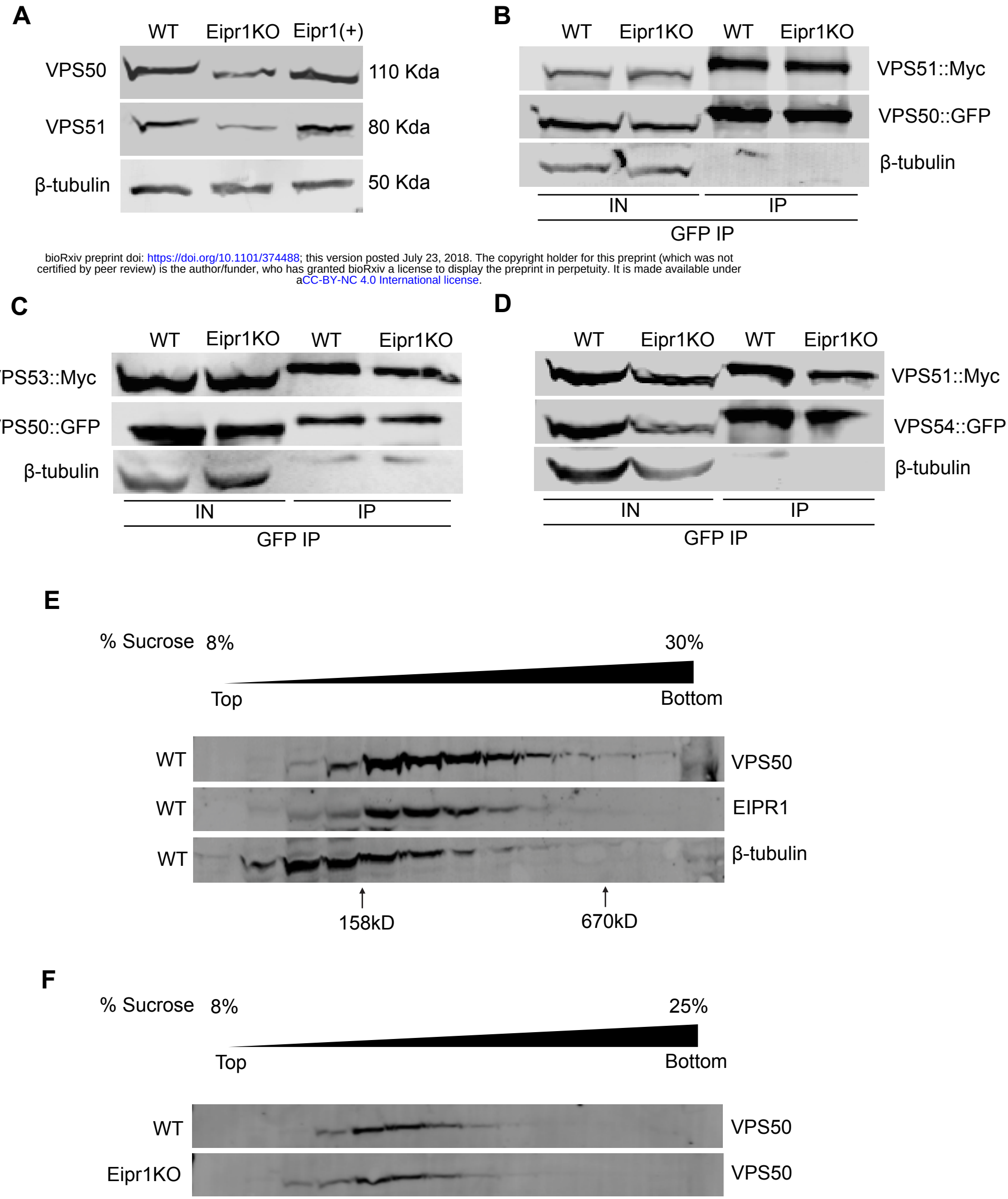

bioRxiv preprint doi: https://doi.org/10.1101/374488; this version posted July 23, 2018. The copyright holder for this preprint (which was not certified by peer review) is the author/funder, who has granted bioRxiv a license to display the preprint in perpetuity. It is made available under aCC-BY-NC 4.0 International license.

Figure 6

A

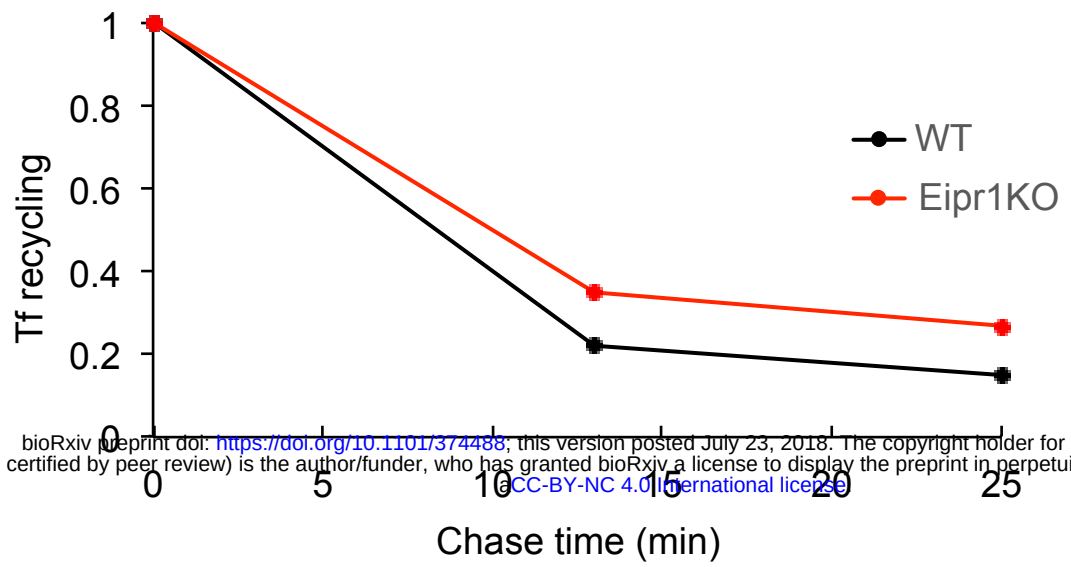

bioRxiv preprint doi: https://doi.org/10.1101/374488; this version posted July 23, 2018. The copyright holder for this preprint (which was not certified by peer review) is the author/funder, who has granted bioRxiv a license to display the preprint in perpetuity. It is made available under CC-BY-NC 4.0 International license.

B

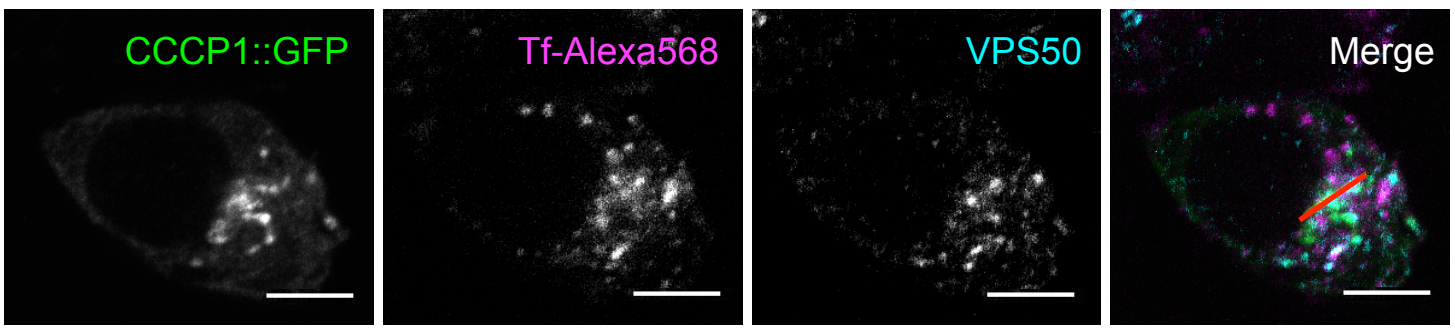

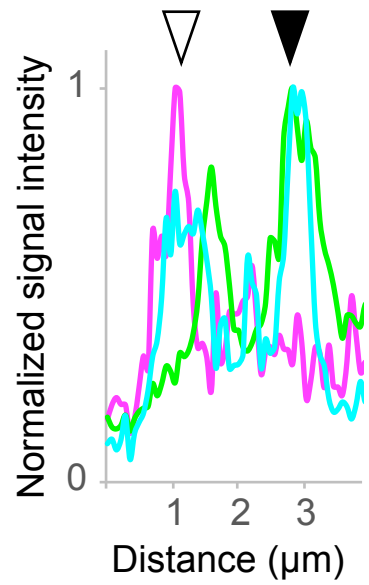

Figure S1

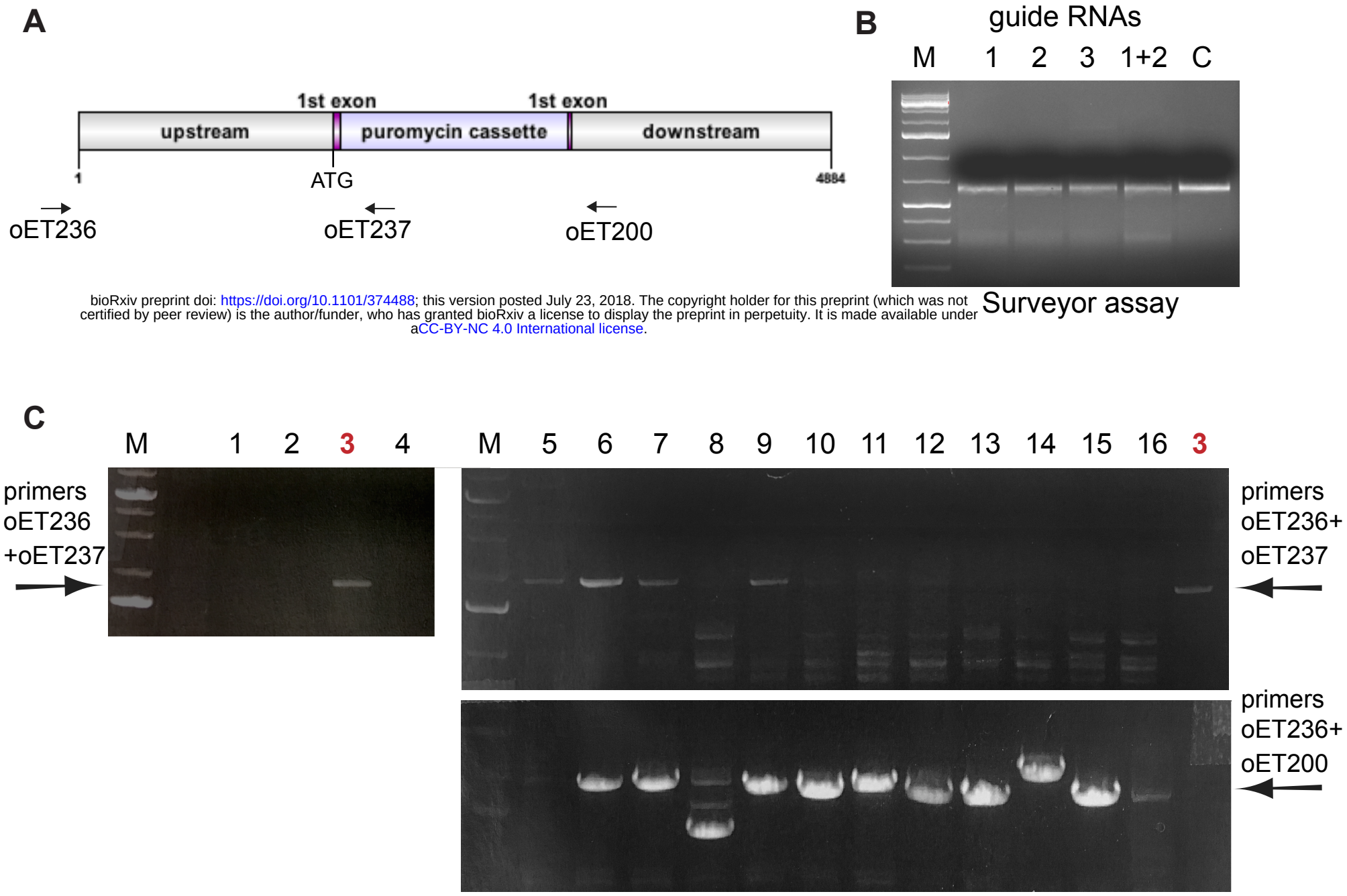

bioRxiv preprint doi: https://doi.org/10.1101/374488; this version posted July 23, 2018. The copyright holder for this preprint (which was not certified by peer review) is the author/funder, who has granted bioRxiv a license to display the preprint in perpetuity. It is made available under aCC-BY-NC 4.0 International license.

Figure S2

A

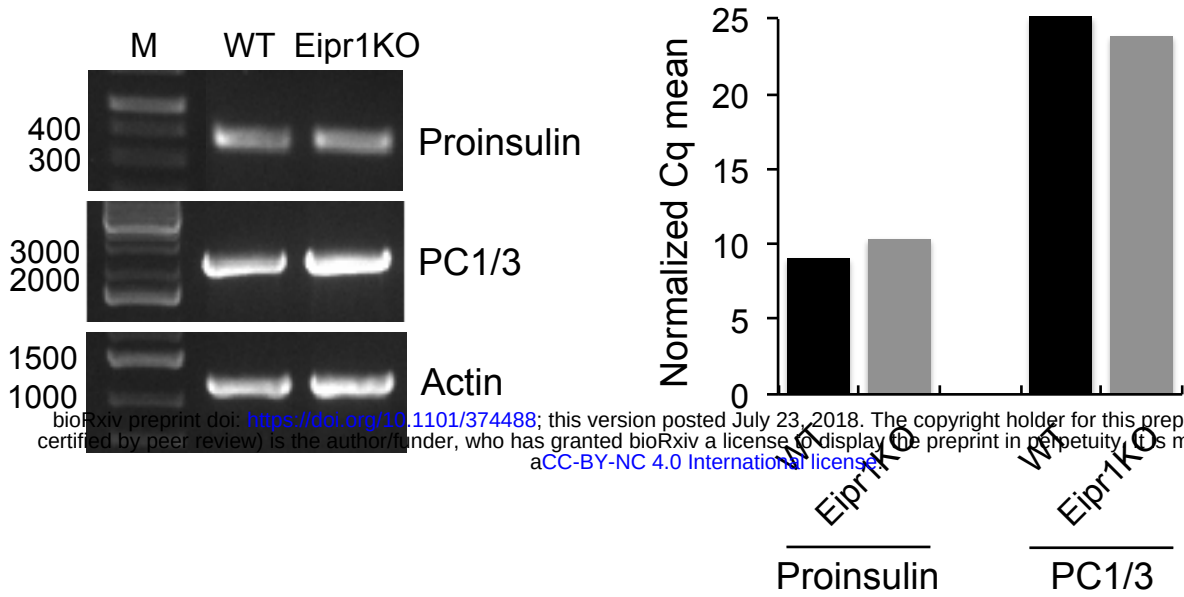

bioRxiv preprint doi: https://doi.org/10.1101/374488; this version posted July 23, 2018. The copyright holder for this preprint (which was not certified by peer review) is the author/funder, who has granted bioRxiv a license to display the preprint in perpetuity. It is made available under aCC-BY-NC 4.0 International license.

B

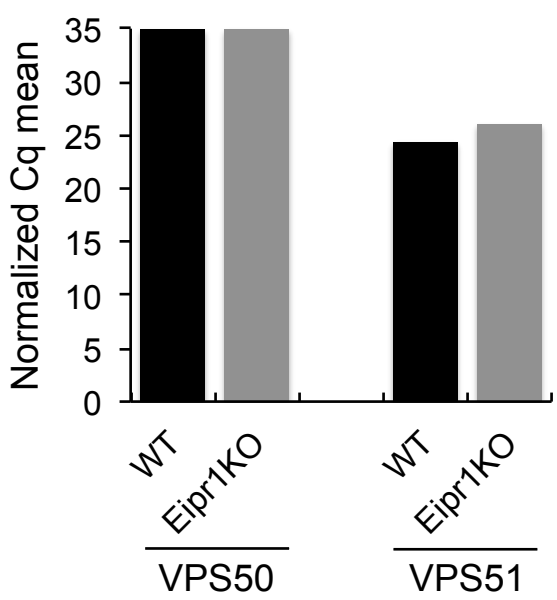

Figure S3

A

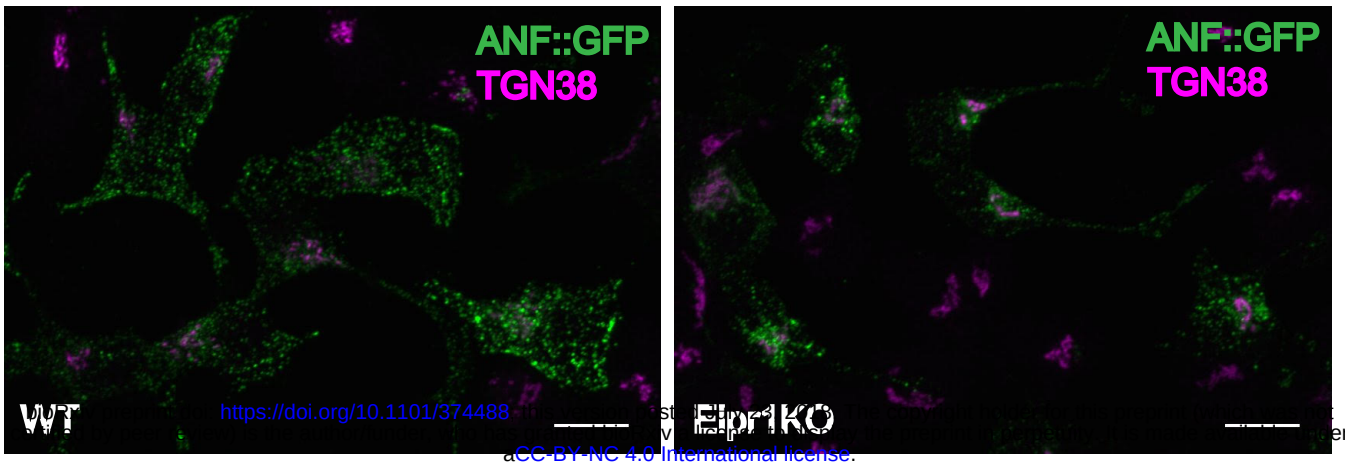

https://doi.org/10.1101/374488
CC-BY-NC 4.0 International license.

B

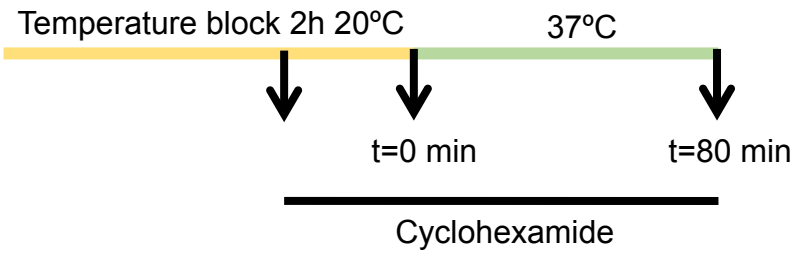

C

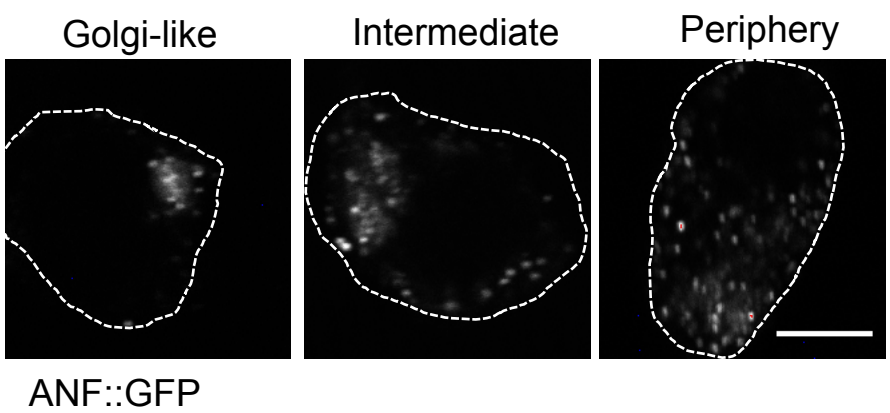

D

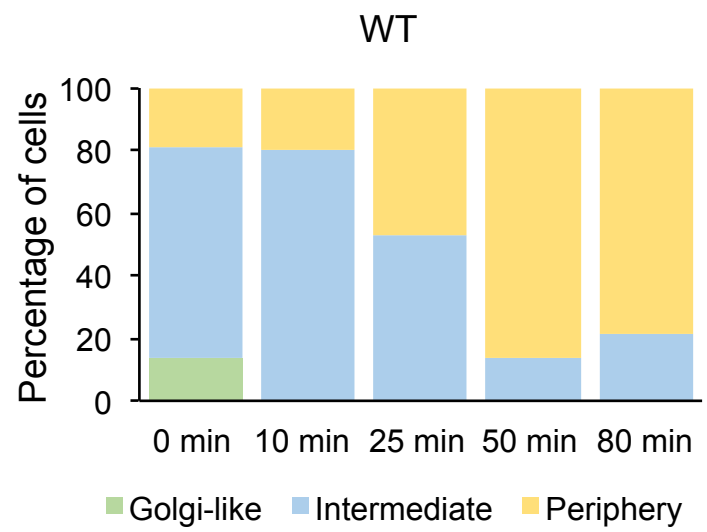

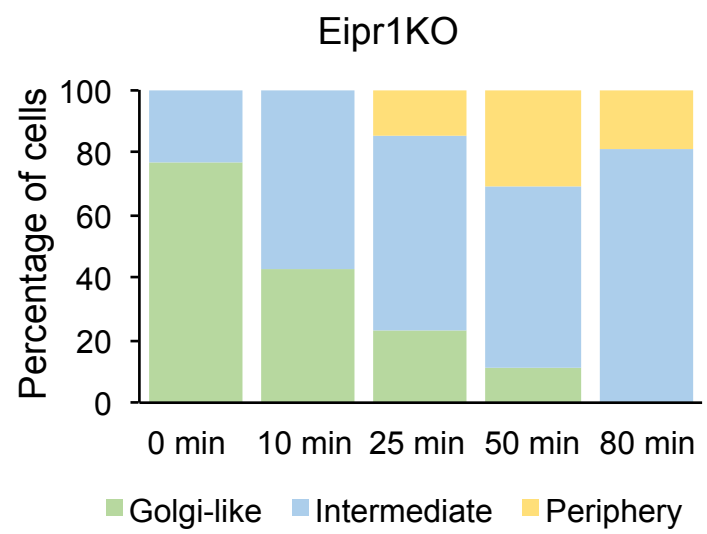

Figure S4

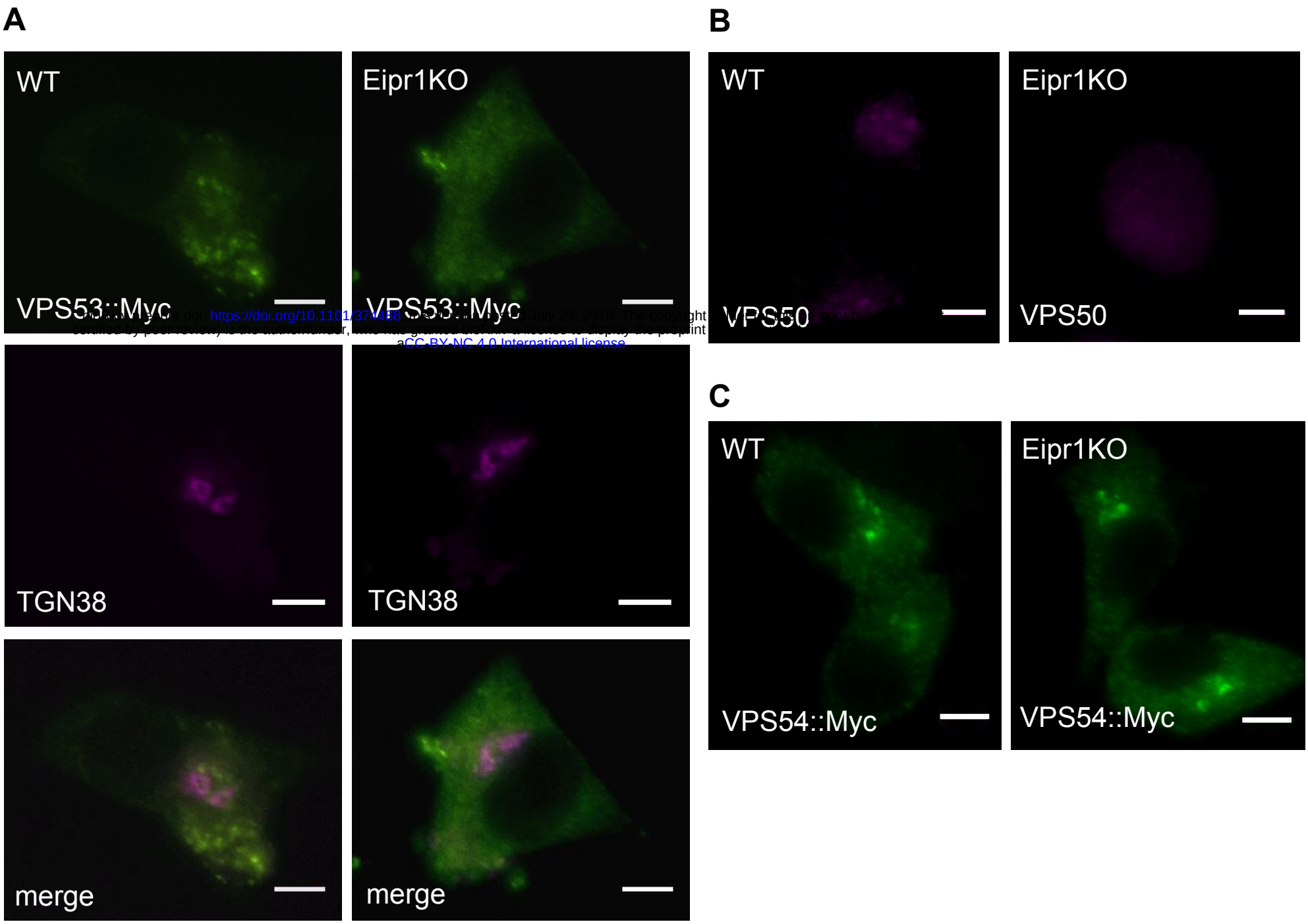

https://doi.org/10.1101/374488 July 23, 2018. The copyright
CC-BY-NC 4.0 International license

Figure S5

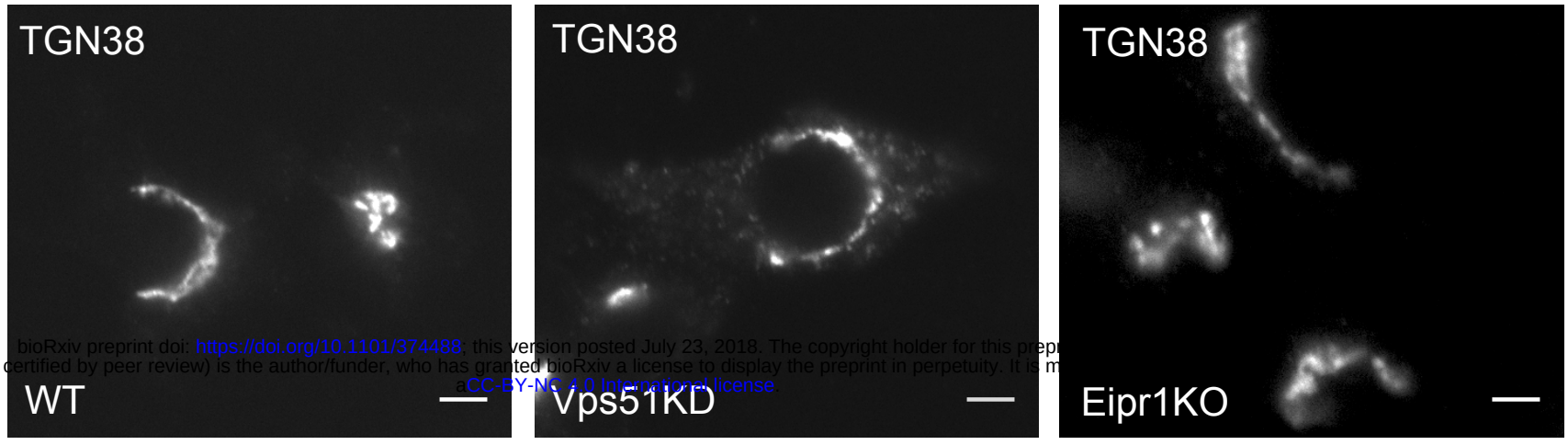

bioRxiv preprint doi: https://doi.org/10.1101/374488; this version posted July 23, 2018. The copyright holder for this prepr
certified by peer review) is the author/funder, who has granted bioRxiv a license to display the preprint in perpetuity. It is m
a CC-BY-NC 4.0 International license.